UNIVERSITY OF CALIFORNIA,
IRVINE

Rare Earth Separation Using Monazite and Xenotime

THESIS

submitted in partial satisfaction of the requirements
for the degree of

MASTER OF SCIENCE

in Materials Science and Engineering

by

Joanne Leadbetter

Thesis Committee:
Professor Martha Mecartney, Chair
Associate Professor Mikael Nilsson
Professor James Earthman

2016

DEDICATION

To

my parents and friends

and also coffee

TABLE OF CONTENTS

Page

LIST OF FIGURES

LIST OF TABLES

ACKNOWLEDGMENTS

I would like to express the deepest appreciation to my committee chair, Professor Martha Mecartney. Without her guidance and persistent help this dissertation would not have been possible.

I would like to thank my committee members, Professors Mikael Nilsson and James Earthman for furthering my education while I focused on research.

I would also like to thank my undergraduate advisor Professor Todd Krauss and mentor Gregory Pilgrim for their confidence in my ability to succeed in graduate school.

Thanks to Kenta Ohtaki and fellow graduate students for their advice and support.

Most of all I wish to express my thanks to my family for their undying support through too many years of school.

ABSTRACT OF THE THESIS

Rare Earth Separation Using Monazite and Xenotime

By

Joanne Leadbetter

Master of Science in Material Science and Engineering

University of California, Irvine, 2016

Professor Martha Mecartney, Chair

A collection of methods to separate rare earth elements are presented here. The first is a two-step separation method using low temperature direct synthesis of monazite followed by a low temperature precipitation of xenotime. Another method presented is a homogeneous precipitation using phytic acid. Both methods were met with limited success, the two step phosphoric acid method shows promise as a rough separation and improves on old fractional crystallization methods. Additionally a method of synthesizing "clean", stoichiometric monazite is presented. Initial results show simply limiting the amount of phosphorous added in a direct precipitation method makes improvements over commercially available $LaPO_4$ without washing with hazardous chemicals.

CHAPTER 1: SEPARATION METHODS FOR RARE EARTH ELEMENTS

1.1 Introduction

1.1.1 Rare Earth Background

Rare earths have become a critical component of the modern material technology scene. They are used in phosphors for color television and flat screens, catalysts, fuel cells, the magnets of electric motors and wind turbines as well as hard drives [1, 2]. Rare earths comprise the lanthanide series as well as yttrium since they occur together in nature. Until 1913 they struggled to be distinguished as individual elements due to their chemical similarity until Henry Moseley used x-ray spectroscopy to observe the individual spectra of the lanthanides, confirming their existence [3].

Rare earths (RE) are not so much rare as they are not found as pure compounds, but clustered together with each other in baestenite, in xenotime or monazite imbedded in gangue material. Ores containing rare earths are not usually found in rich veins as with other valuable materials such as gold or silver, but instead are spread out over a wide area, which is not ideal for mining and processing [4]. Their rarity is compared to other elements found in nature in Figure 1.1, where it shows that these elements are not even as rare as gold [5]. Even after the RE rich ore is collected, extensive processing by solvent extraction are currently employed to separate them into useable forms. Costs are volatile due to demand and the unfortunate geographical distribution. This has recently caused an increase in interest in efficient ways to recycle and separate these elements [6].

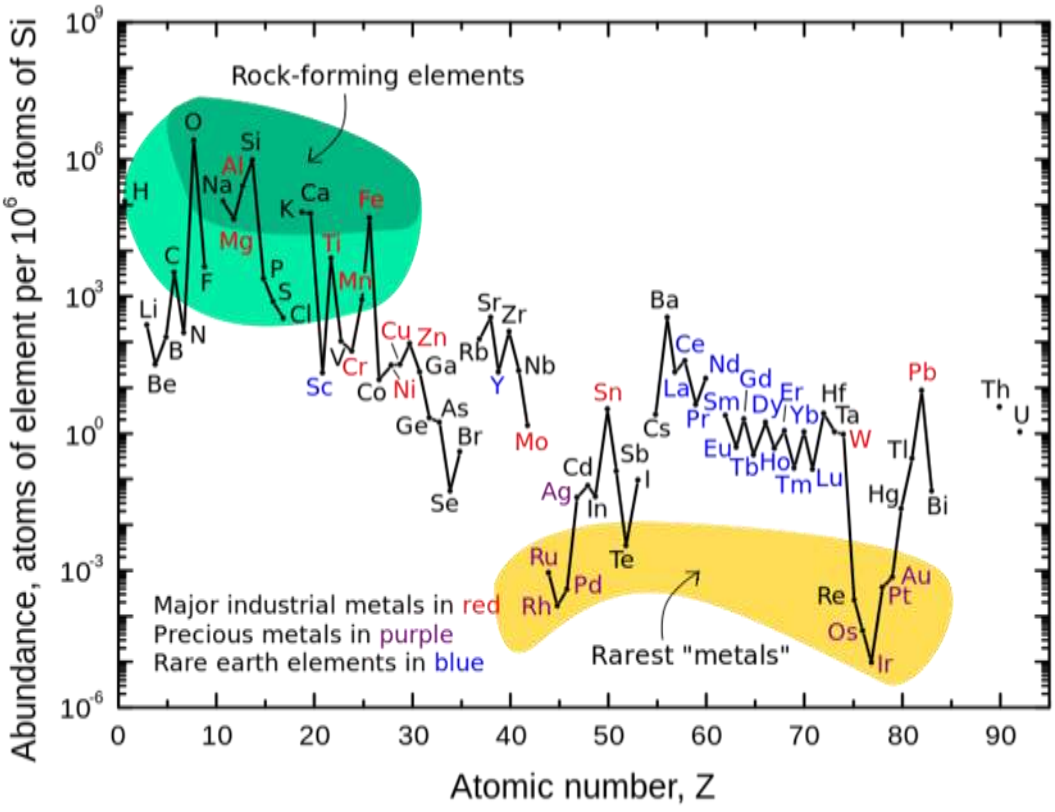

Fig. 1.1: Abundance of naturally occurring elements on earth [5]

However, their rarity does not perfectly correlate to their value. Figure 1.2 shows the price for each rare earth element in oxide form. Notably, this emphasizes the value of heavy rare earth elements.

Fig. 1.2: Rare earth oxide prices per gram (Sigma Aldrich April 27th 2016)

1.1.2 History of Rare Earth Separation Methods

The first technique used to separate rare earth elements was fractional crystallization devised by Charels James in 1906. This involved refining and separating based on small differences in solubility [3]. Due to their extremely similar properties this process was particularly laborious for rare earth separation and involved several iterations [8].

The next major separation technique for rare earth separation, used in the 1940s was ion exchange [9]. In this process a liquid phase mixture of rare earths are run through a column containing an ion exchange polymer resin with either a cationic or anionic polymer. The rare earth compounds then form bonds with the polymer. The strength of these bonds varies with the individual rare earth's properties. A solvent can then be used to elute out the rare earths which travel at different rates based on their bond strength.

The dominate method for separating rare earths since the 1960s, has been liquid-liquid extraction [10]. The ore is separated from the gangue material and processed

through many steps until only trivalent REEs remain. These are separated in a mixing/settling chamber with aqueous and organic phase which divides the REE in a continuous process [11]. Further purification can still be done by ion exchange. Current methods can produce 99.999% purity of most rare earths by solvent extraction [12].

1.1.3 Separation by Different Phases

Other notable modern methods recently proposed include Uda *et al.* [13] separated rare earths by controlled reduction and vacuum distillation. This processes specifically aimed to better separate Pr and Nd, known to be the most difficult to separate by solvent extraction. Recently bacteria have been used to separate rare earths [14].

Schatzmann *et al.* [15] have developed a simple method of synthesizing La-monazite by drop-wise precipitation but does not precipitate xenotime in the presence of Y. It has been observed in nature that monazite preferentially incorporates the larger, lighter rare earth elements (LREE La-Gd) while xeotime takes the smaller, heavier rare earth elements [7]. Monazite is formed at high temperature with rare earths La to Eu [16]. This method has potential as an early step in the separation process if it can precipitate the light elements in their preferred, monazite structure and leave the heavy rare earths in the liquid phase for decanting. This liquid phase can then be precipitated under dilute conditions to form xenotime or churchite or further processed into an oxide.

The chemical similarity of the rare earths makes them difficult to separate by traditional means. They have only slight differences in ionic radius, electronegativity and valence. One of the major differences between the rare earths and lanthanide series is their preference for eight or nine fold geometries. The so called light rare earth elements (LREE)

from La to Gd prefer nine fold monazite structure while the heavy rare earth elements (HREE) prefer the eight fold xenotime structure based on their ionic radii [7].

Since the rare earths can be divided by their preferential crystal structures as shown below in Figure 1.3, and the value of each element is heavily skewed towards the heavy rare earths as previously established in Figure 1.2, a method that took advantage of this difference to divide up these elements quickly would have potential applications in industry.

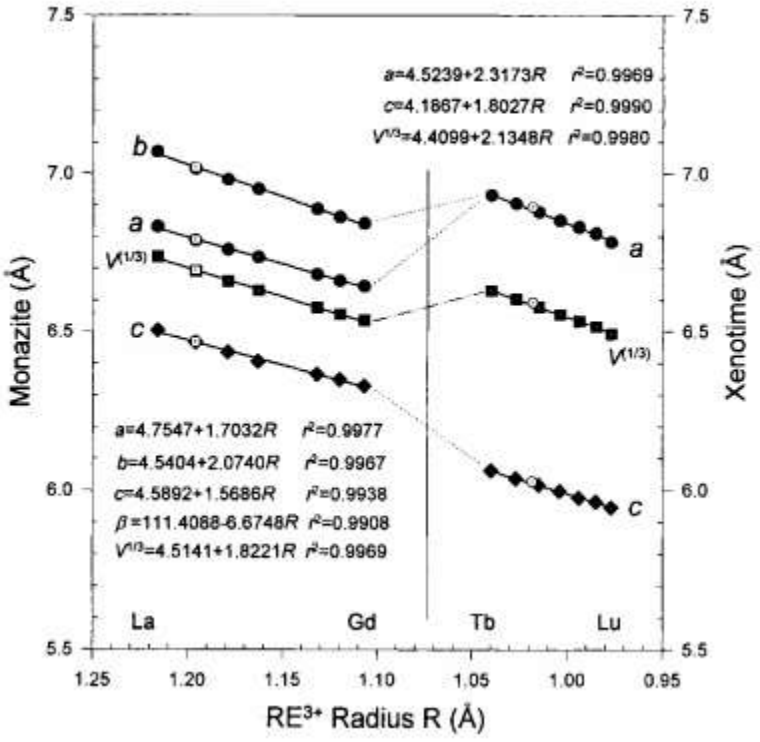

Fig. 1.3: Variation of lattice parameters with RE element for Synthetic RE(P04) phases. [1.7]

1.1.4 Crystal Structures

Since rare earths are found in nature as monazite and xenotime it is necessary to explore their crystal structure and chemistry in addition to their hydrate forms. Though their hydrates are less commonly found in nature, many synthetic routes produce the hydrate as an intermediate.

Monazite minerals have the ideal formula of $RE(PO_4)$ where the most common REE are the lighter half of the lanthanides. It has the space group $P2_{i/n}$ with equal number of PO_4 and REO_x polyhedral. The most distinct feature of its crystal structure is its 9 fold coordination. [7]

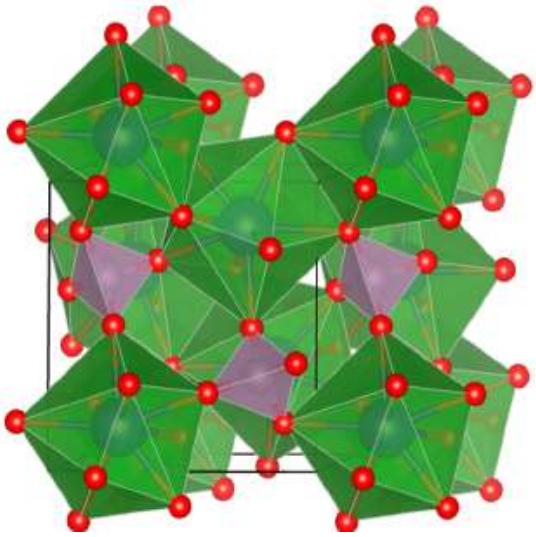

Fig. 1.4: Crystal Structure of Monazite

Rhabdophane has the orthorhombic, P222 structure and an ideal formula of $(RE)PO_4\ 6H_2O$, containing the same light rare earths as monazite. It is thought that dehydration occurs between 100 and 400^oC and then phase change to monazite takes place between 500 and 900^oC [17]

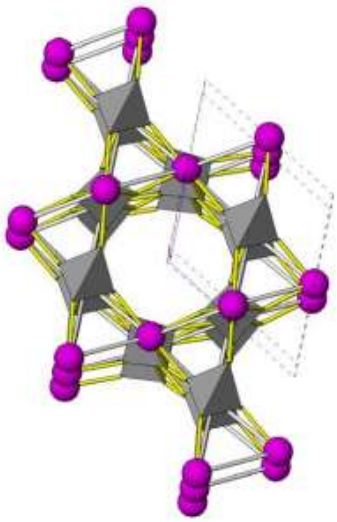

Fig. 1.5 Crystal structure of rhabdophane

Xenotime, compared to monazite has a much more regular 8 fold coordination but the same ratio of rare earth to phosphate. This takes the same formula $RE(PO_4)$ but tends to incorporate the heavy rare earths with smaller atomic radii. [18]

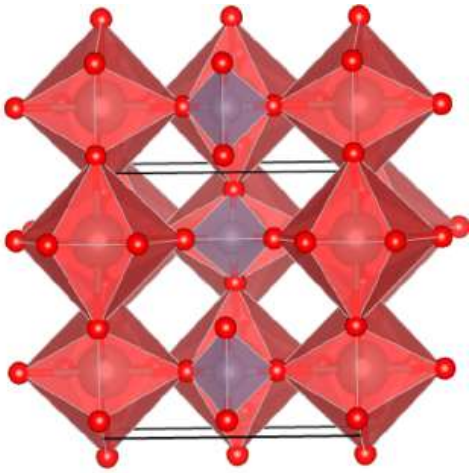

Fig. 1.6 Crystal structure of xenotime

The mineral form of churchite – (Y) is a rare earth hydrated phosphate with ideal formula $YPO_4 \bullet 2H_2O$ which can contain erbium and other late lanthanides [18]. It has a

monoclinic symmetry with space group I2/a [19]. Churchite is the hydrate of the previously mentioned xenotime structure.

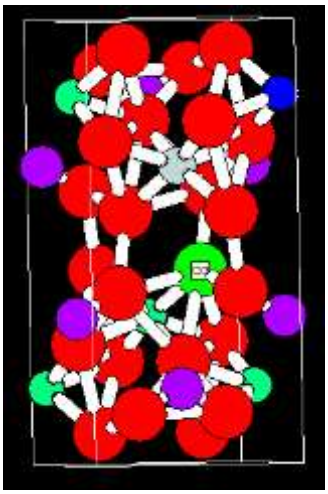

Fig. 1.7 Crystal structure of churchite

1.1.5 Phytic Acid

Phytic acid (1,2,3,4,5,6 hexakis (di-hydrogen phosphate) myo-inositol) is a polydibasic acid ester that is found in the shells of nuts and plant seeds seen in Figure 1.8. In nature it acts as the primary storage of phosphorous in the plant tissue in which it is found. Phytic acid binds strongly to iron, zinc and calcium which can interfere with the availability of nutrients and vitamins if consumed [20]. Additionally it acts as an energy store, cation source and myoinositol source. During commercial processing and manufacturing of foods it is discarded as a waste product and can thus be obtained cheaply in large quantities if so desired [21].

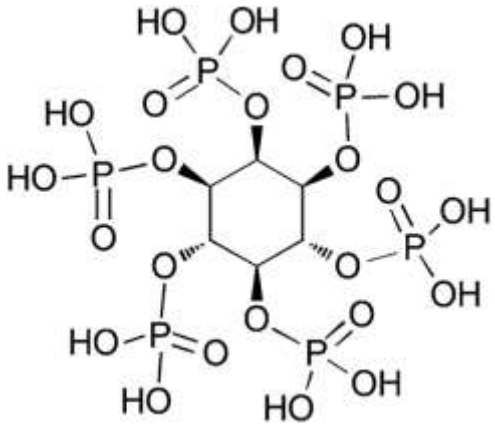

Fig. 1.8: Phytic acid structure

The molecule undergoes hydrolysis of the phosphor-ester linkages in solution at elevated temperatures leading to the formation of inositol and freeing hydrogen phosphate species.

Rare earths and other M^{3+} metals form metal phosphors, displacing hydrogen ions leading to a drop in pH. In turn the phytic acid molecules would release water molecules would could result in an ultimately endothermic reaction. Though this could be slowed by the presence of sodium ions which phytic acid bids to preferentially. According to Siddiqi *et al.* [22] the calculated order of stability is $Ho^{3+} > Dy^{3+} > Tb^{3+} > Sm^{3+} > Gd^{3+} > Nd^{3+} > Pr^{3+} > Ce^{3+}$.

This difference in stability suggests that a very slow, careful reaction with mixed rare earths in phytic acid has the potential to be a separation method by fractional crystallization. If this could be controlled by either temperature, pH, or presence of sodium ions could control the conditions well enough to only precipitate one rare earth at a time, one could collect the precipitant and then further alter the conditions to precipitate the next element as a phosphate compound.

1.1.6 Rare Earth Separation Objectives

To this effect, methods have been investigated to use monazite and xenotime as preferential crystal structures to separate heavy and light earth elements. The first method involves using low temperature monazite precipitation to quickly gather the light earth elements as precipitant and the heavy rare earths in the liquid phase to be further separated. The second uses phytic acid to homogeneously separate rare earths in hopes of being able to vary conditions in a slow precipitate different crystal structures or rare earths.

1.2 Rare Earth Separation by Direct Precipitation with Phosphoric Acid

1.2.1 Direct Precipitation Separation Methods

A solution of 85% phosphoric acid was heated in a 100mL beaker on a hot plate to 150^{o}C measured in solution by temperature probe in order to evaporate the excess water shown in Figure 1.9. Once the condensation on the glass disappeared (about 30 mins) the solution was heated or cooled to the target temperature for the experiment, 100, 125, 150, 175 or 200^{o}C. A 1:1 molar ratio solution of $Y(NO_3)_3$ (4.7g, 0.0025 mols) and $La(NO_3)_3$ (5.3 g, 0.0025 mols) dissolved in the minimum amount of water was added drop-wise to the heated acid while stirring.

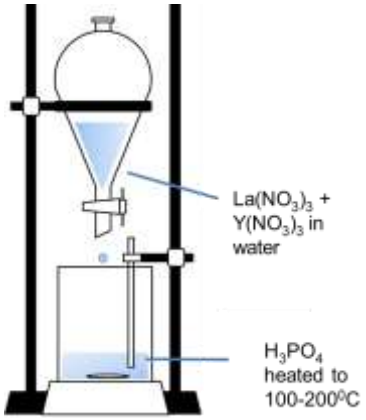

Fig. 1.9: Experimental setup separation using phosphoric acid

After the first drop the acid solution turned orange yellow, then precipitation was observed after ten minutes and about half of the mixed rare earth solution was added. As the reaction progressed the solution turned milky white and orange bubbles formed and were released as visible orange gas. Once the solution stopped producing colored glass and was a milky white color, samples were separated by hot centrifuge. The collected white precipitant was then were washed with di water several times to a pH of 7 and dried with acetone to prevent clumping.

The liquid phase was transferred to a 500 mL Erlenmeyer flask and diluted 250x with di water. This solution was then heated to 75°C for about 24 hours and lumpy white powder formed. For higher initial temperature (ie 200°C) formation was slower and produced less powder. Powder was centrifuged and washed as previously described. This procedure is outlined in flow chart in Figure 1.10.

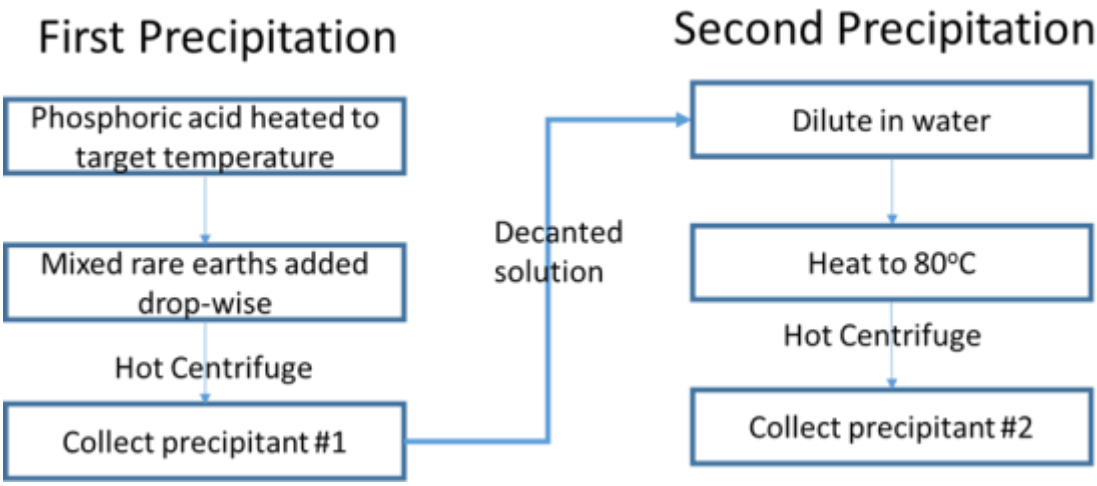

Fig. 1.10: Procedure diagram

Additional experiments were performed on excess decanted liquid phase. In these experiments liquid concentrated ammonia was added to 10x diluted decanted liquid after hot centrifuge separation. This resulted in immediate white precipitation and was washed to pH 6.5 with water and dried with ethanol and acetone.

Collected powders were examined and characterized by XRD X-ray diffraction (Rigaku SmartLab X-ray diffractometer) and SEM (FEI Magellan 400 XHR SEM). Further analysis of structure and composition was carried out by energy dispersive X-ray spectroscopy (EDS Oxford Instruments 80mm2) and Rietveld refinement (PDXL).

1.2.2 Direct Precipitation with Phosphoric Acid for Separation of Rare Earths

Yields of the initial precipitation were collected by weighing initial powder collected after washing assuming all $LaPO_4$ monazite formed. Calculated values are shown in Table 1.1.

Table 1.1: Yield of initial precipitation of monazite powder at initial precipitation temperatures.

Temperature (°C)	Yield
200	60%
175	79%
150	58.8%
125	22.5%
100	28.1%

The initial precipitation was examined by SEM and XRD. Figure 1.11 represents the range of shapes found in the first step of the separation from higher and lower temperatures. The floral, platted particle bundles tend to become rounder and decrease in size with temperature. The surface of the particles has a bumpy texture which seems more defined at lower temperatures.

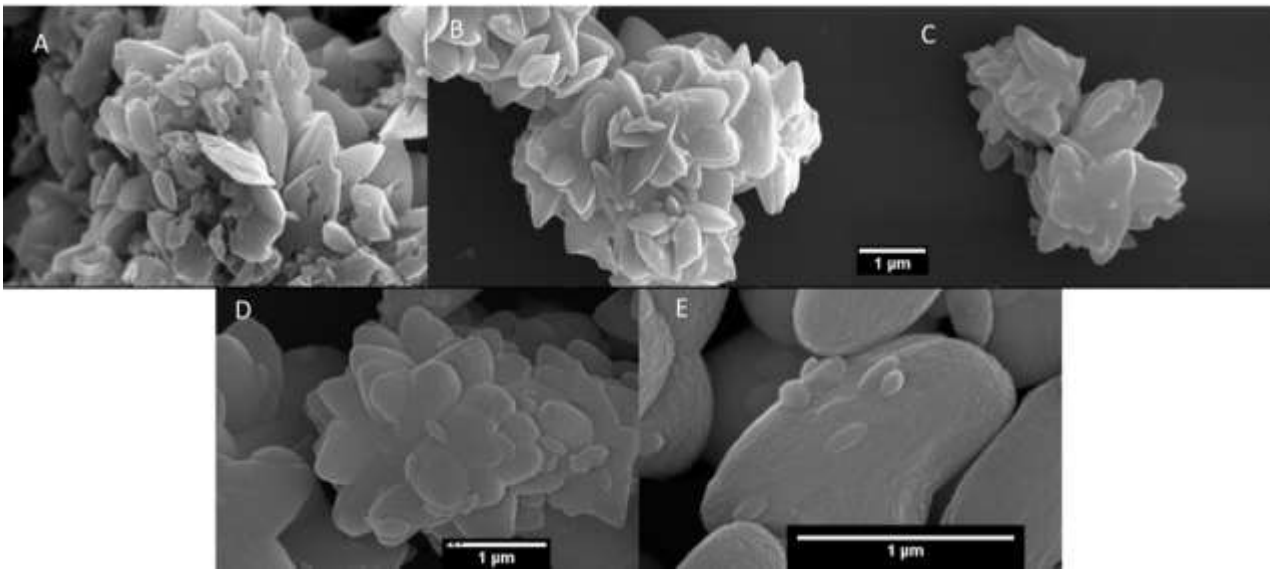

Figure 1.11: Initial precipitation of monazite formed A) 200°C, B) 175°C, C) 150°C, D) 125°C, E) 100°C in phosphoric acid on Si wafer.

XRD was taken of the powders and matched monazite structure as shown in Figure 1.12. When peaks were compared with the XRD pattern of a sample prepared with only

lanthanum there was a small shift to the right, suggesting a decrease in unit cell volume which may be due to the incorporation of yttrium into the lanthanum monazite unit cell.

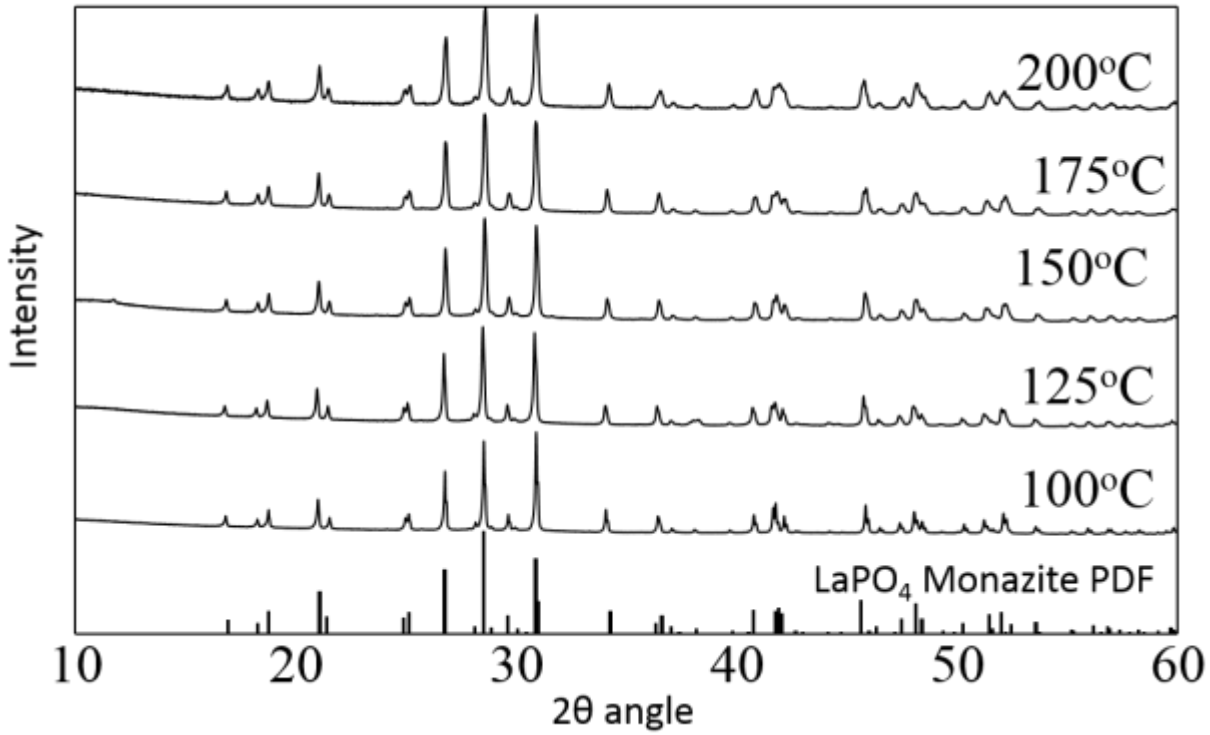

Figure 1.12: Characterization of crystal structure from initial precipitation temperature range 100-200°C by XRD matched to $LaPO_4$ monazite.

The shift in two theta angle is not obvious when looking at the full spectra of precipitant, however Figure 1.13 below makes it more apparent. It is important to note that the line at 28.6 2θ represents the PDF card of monazite (01-083-0651).

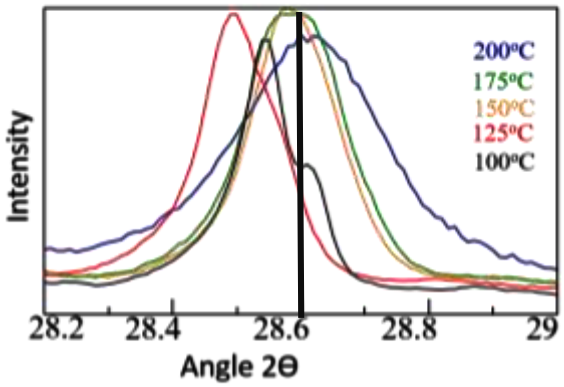

Figure 1.13: Overlap comparison of all synthesized monazite powder from 200 to 100°C using the main peak of monazite at (120) 28.6 degrees

Lower temperatures, 100 and 125°C seem to shift to lower angles while higher are very close or higher to the PDF card data presented. To further quantify the shift in 2Θ angle, Reitvelt refinement for each temperature was carried out and shown in Table 1.2 below. This data was compared with the unit cell volume and parameters of the standard pdf card for LaPO4 monazite (01-083-0651).

Table 1.2: Unit cell volumes by Reitvelt refinement of initial monazite precipitation and heavy rare earth precipitation compared to standard.

Temperature (°C)	a(A)	b(A)	c(A)	alpha(°)	beta(°)	gamma(°)	V(A^3)
Monazite PDF	6.8250	7.0570	6.4820	90	103.21	90	303.938
100	6.8429	7.0755	6.4990	90	103.21	90	306.343
125	6.8527	7.0774	6.5254	90	103.79	90	307.353
150	6.8425	7.0645	6.5176	90	103.73	90	306.042
175	6.8353	7.0641	6.5198	90	103.71	90	305.842
200	6.8306	7.0628	6.4873	90	103.21	90	304.696

Reitvelt refinement shows a general downward trend in unit cell volume with increasing temperature moving closer to the reported PDF card standard used for monazite; but erratic trends in individual directions in the unit cell. Figure 1.14 below serves to emphasis the

relationship described by the data shown in Table 1.2. However the error was more than 10% of the values which overlaps with all of the data points.

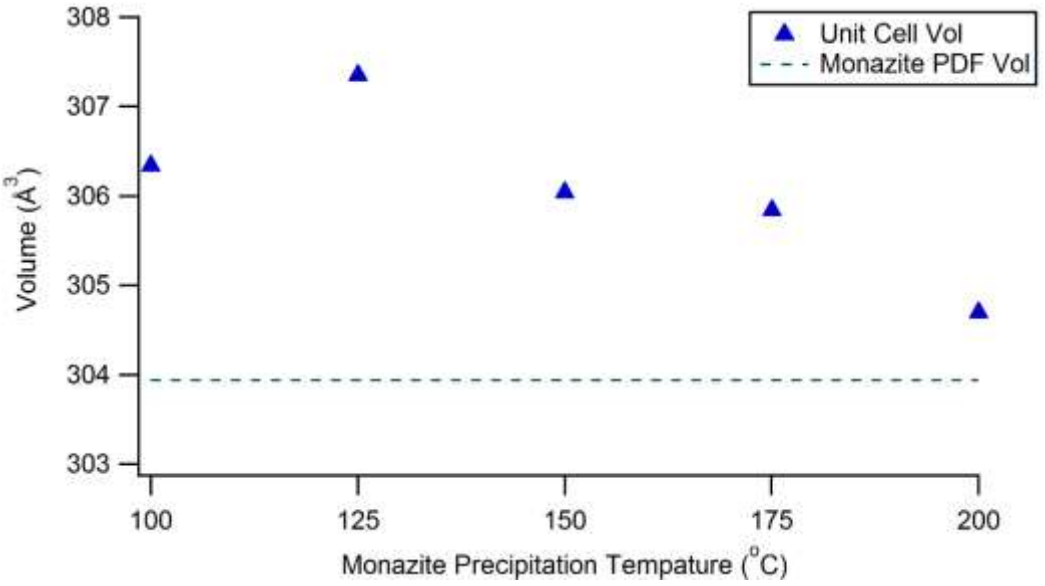

Figure 1.14: Unit cell volume of initial precipitation of monazite with La at different temperature compared to the monazite PDF card volume.

1.2.3 Second Step of Separation, Precipitation of Decanted Solution at 80°C

After the monazite powder had been collected, after precipitation and separation, the remaining liquid layer was diluted and heated to 80°C. White powder formed after about an hour and was collected and washed. Yields were taken by weighting collected powders after thoroughly drying and compared against xenotime theoretical yield and reported in Table 1.3.

Table 1.3: Yield of rare earths after precipitation at 80°C from the second part of separation listed by initial separation temperature

Initial Temperature	Crystal Structure	Yield
200	Monazite	21%
175	Xenotime	33%
150	Xenotime	35%
125	Rhabdophane	57%
100	Monazite	79%

SEM imaging was done on the decanted, precipitated powders dispersed on Si wafers Figure 1.15 represents the range of shapes found in the first step of the separation from higher and lower temperatures. The powders show much more variety than the initial monazite precipitation. There are rounded clusters and even globby smaller particles smeared in the background.

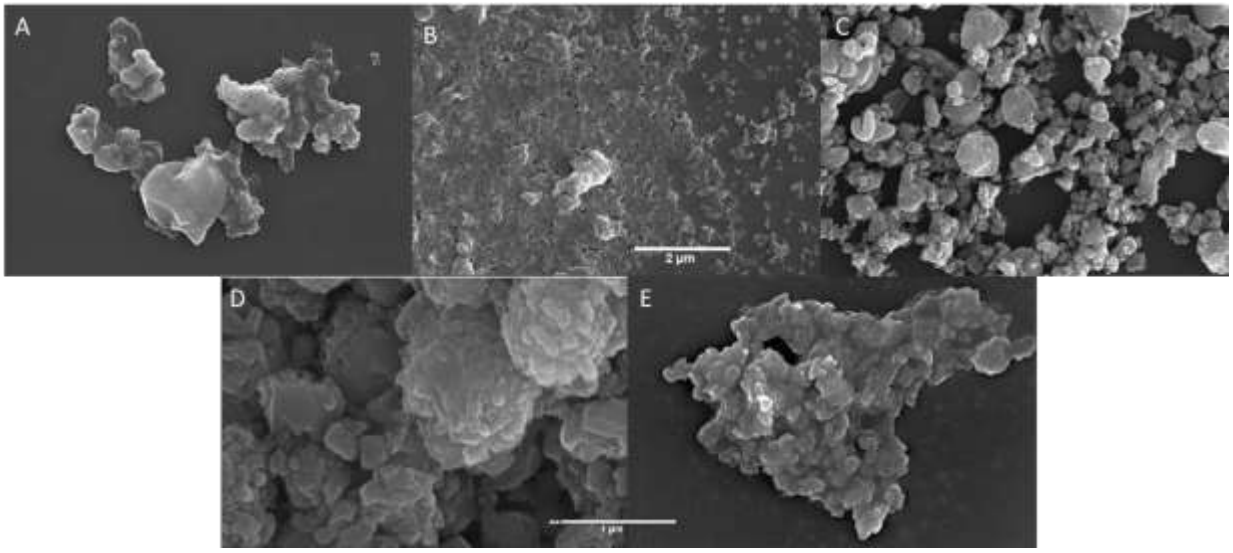

Figure 1.15: Second step precipitation at 80°C from initial precipitation of monazite at A) 200°C, B) 175°C, C) 150°C, D) 125°C, E) 100°C on Si wafer.

Powder XRD was used to determine the structure of the collected powder. Figure 1.16a -1.16e identifies the range of crystal structures from monazite to xenotime to rhabdophane.

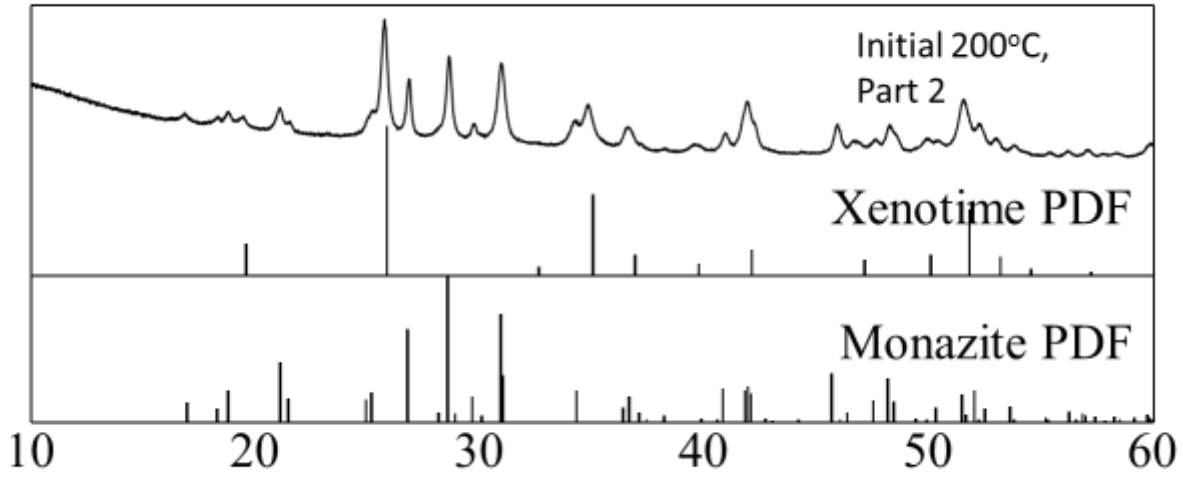

Figure 1.16a: XRD of heavy rare earth precipitation from the liquid pour off after the initial monazite separation at 200°C , crystalized in dilute solution

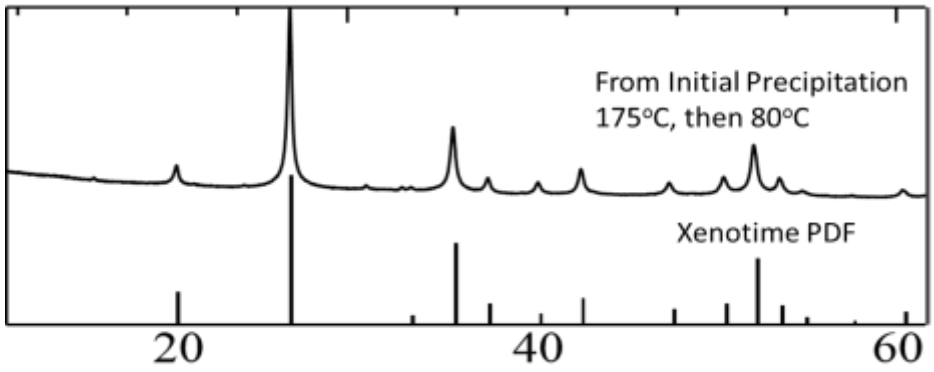

Figure 1.16b: XRD of heavy rare earth precipitation from the liquid pour off after the initial monazite separation at 175°C , crystalized in dilute solution

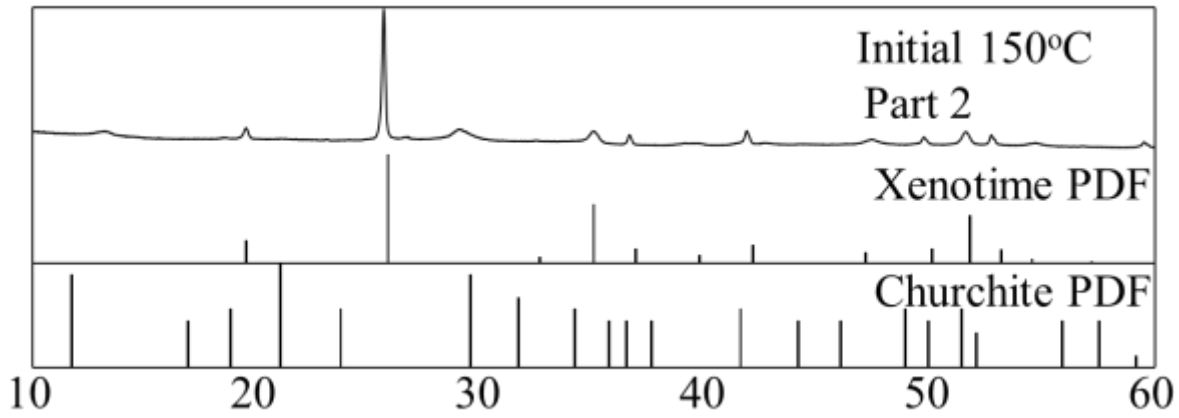

Figure 1.16c: XRD of heavy rare earth precipitation from the liquid pour off after the initial monazite separation at 150°C , crystalized in dilute solution

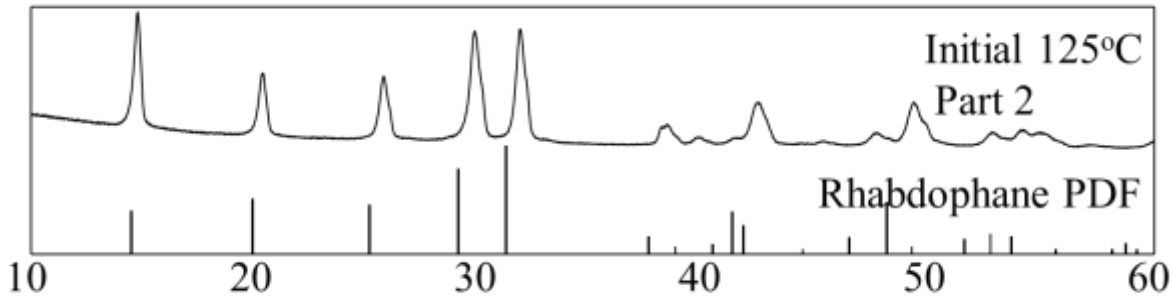

Figure 1.16d: XRD of heavy rare earth precipitation from the liquid pour off after the initial monazite separation at 125°C , crystalized in dilute solution

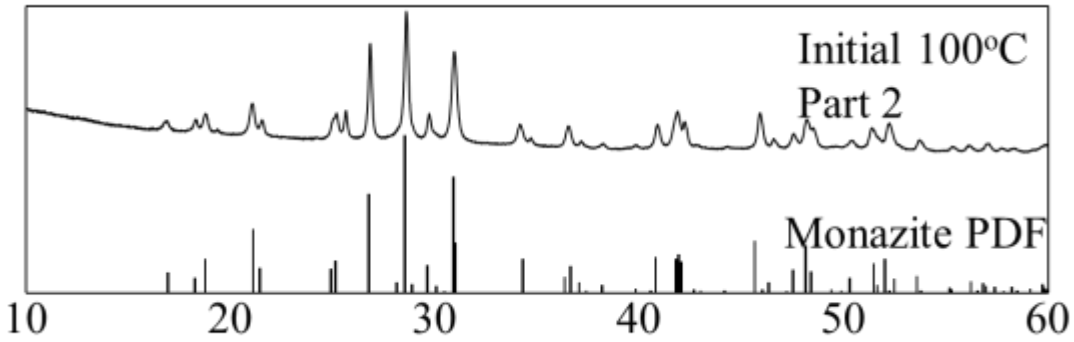

Figure 1.16e: XRD of heavy rare earth precipitation from the liquid pour off after the initial monazite separation at 100°C , crystalized in dilute solution

In order to assess the effectiveness of the separation the amount of Y in the initial precipitation and the amount of La in the liquid decanted. The ratio of Y to La was measured by EDS on the SEM as displayed in Table 1.4.

Table 1.4: EDS data of initial precipitation and second 80°C precipitation.

Temp (°C)	Initial Separation %Y in the La sites	Decanted solution at 80C % La in the Y sites
200	10	3.2
175	10	5.4
150	8.9	4.9
125	5.5	28
100	6.8	58

The first step of the separation all had a similar ~10% incorporation of Y but a hi at lower temperature.

1.2.4 Ammonia Precipitation From Initial Phosphoric Acid Precipitation

In addition to the decanted, diluted and heated to 80°C second step precipitation, an alternate route was also investigated. This invlolved simply adding ammonia to the decanted solution. The endothermic reaction produced a white precipitant immediately. SEM was used to examine the produced material in Figure 1.14 below.

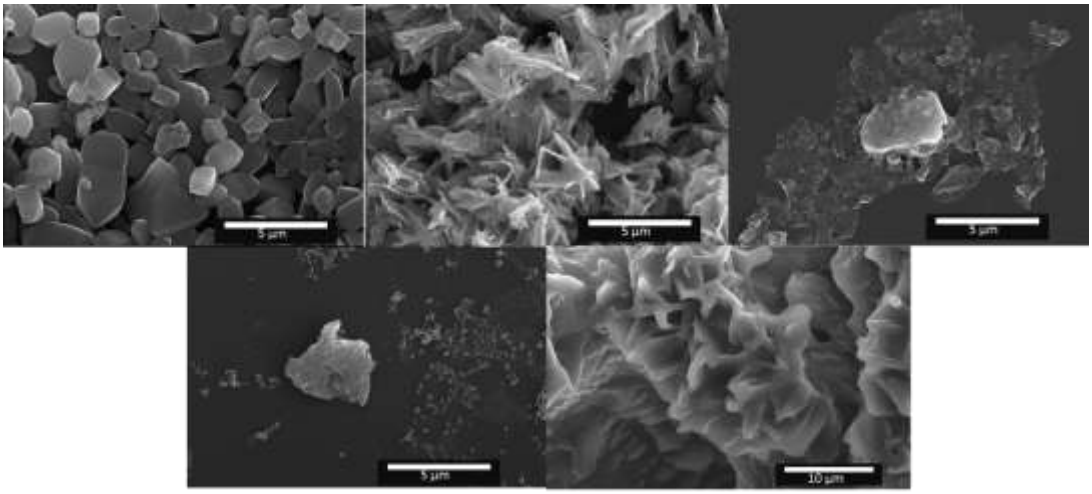

Fig. 1.17: SEM of ammonia precipitant from 100-200°C dispersed on Si wafer

This series of powders were then examined by XRD below in Figure 1.17. The powder was either amorphous or matched the bisphorophosphammite structure.

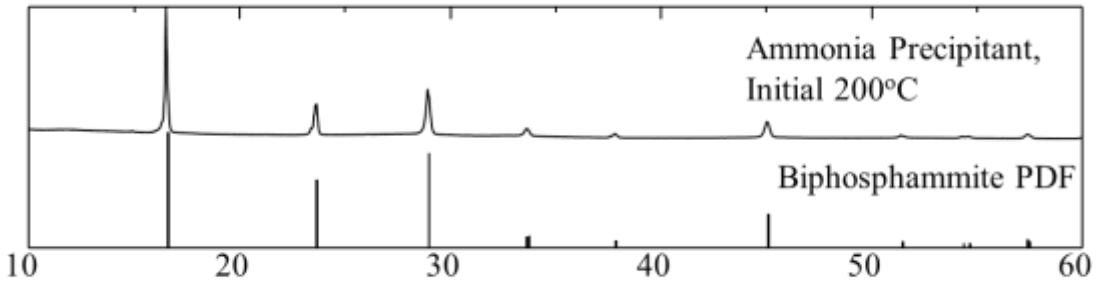

Fig. 1.18a: XRD of heavy rare earth precipitation from the liquid pour off of the initial separation at 200°C , precipitated with ammonia solution

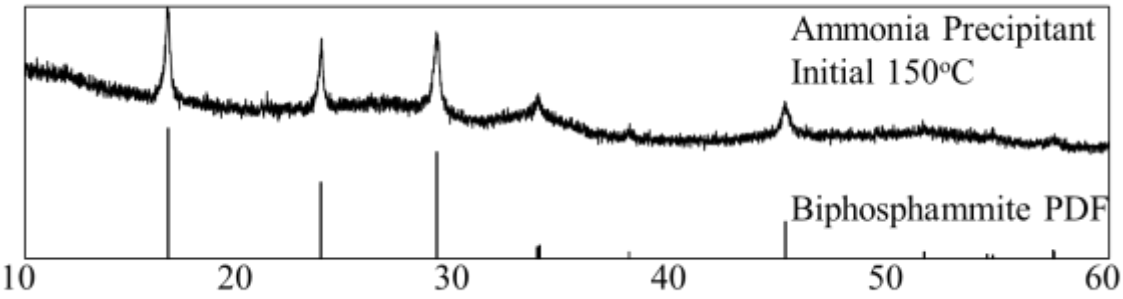

Fig. 1.18b: XRD of heavy rare earth precipitation from the liquid pour off of the initial separation at 150°C , precipitated with ammonia solution

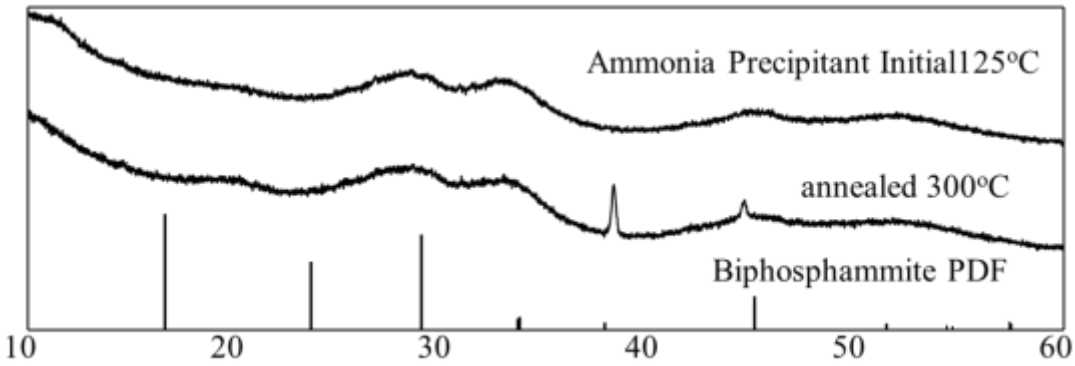

Fig. 1.18c: XRD of heavy rare earth precipitation from the liquid pour off of the initial separation at 125°C , precipitated with ammonia solution.

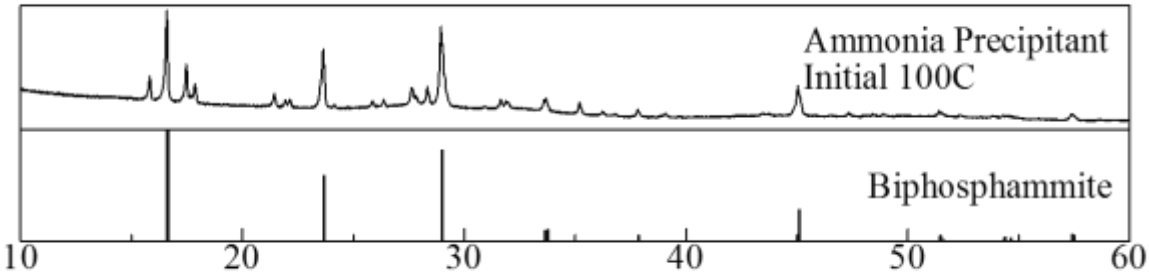

Fig. 1.18d: XRD of heavy rare earth precipitation from the liquid pour off of the initial separation at 100°C , precipitated with ammonia solution

1.2.3 La and Dy Experiments

Further experiments were done to test the phase separation technique using lanthanum and dysprosium. The first step was done at 150°C because the range between 150 and 175°C had the best separation factor for the heavy rare earths. The resulting powered was examined by SEM in Figure 1.19. Morphology of the resulting initial powder showed characteristic rice-like morphology previously seen in monazite precipitants. The second precipitation at 80°C was also similar to the previous La-Y system studied.

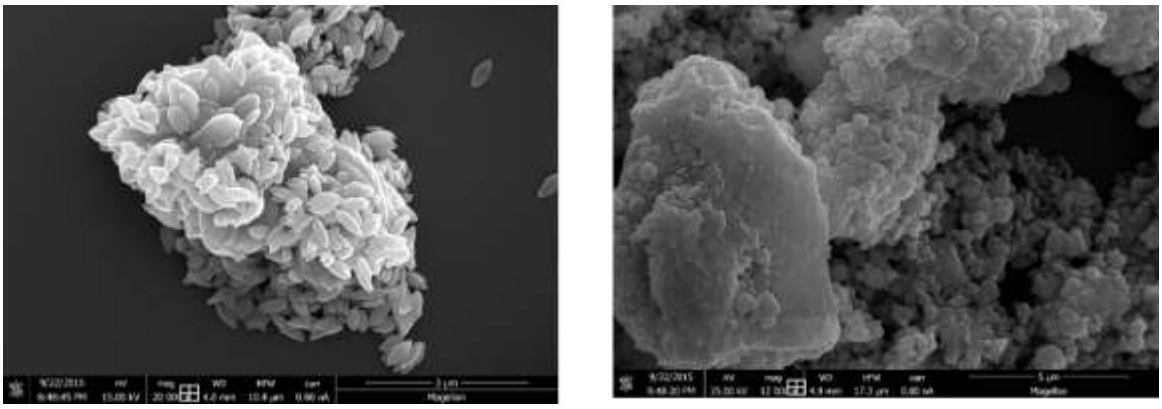

Fig. 1.19: SEM of a) monazite precipitated with La and Dy at 150°C and b) the second step precipitation at 80°C

Composition data was collected with EDS and presented in Table 1.5 below. Reported is the 150°C La-Dy separation as well as an initial attempt at a 9La to 1Dy ratio separation to more closely resemble a rare earth system that might be found in nature.

Table 1.5: La-Dy initial monazite precipitation and second step at 80°C

	Initial Separation %Dy in the La sites	Decanted solution at 80C %La in the Dy sites
150°C	5	30
9La:1Dy	15	18

XRD spectra was also collected in order to confirm the crystal structures produced by the separation synthesis in Figure 1.20 and 1.21. Similar to previous experiments; initial precipitation matches monazite and the second precipitation at 80°C matches rhabdophane.

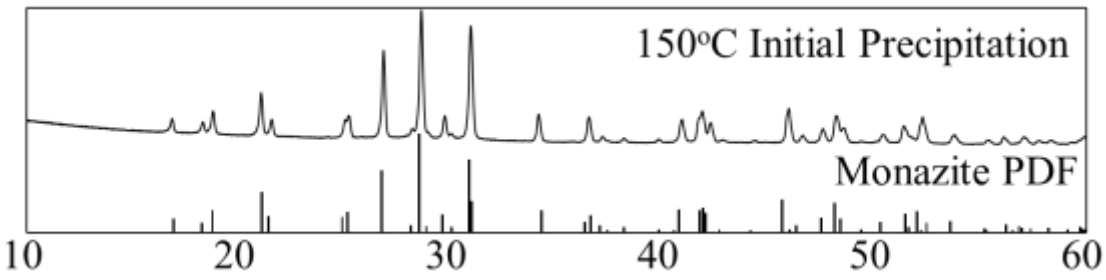

Fig. 1.20: XRD spectra of initial monazite precipitation from La-Dy system at 150°C

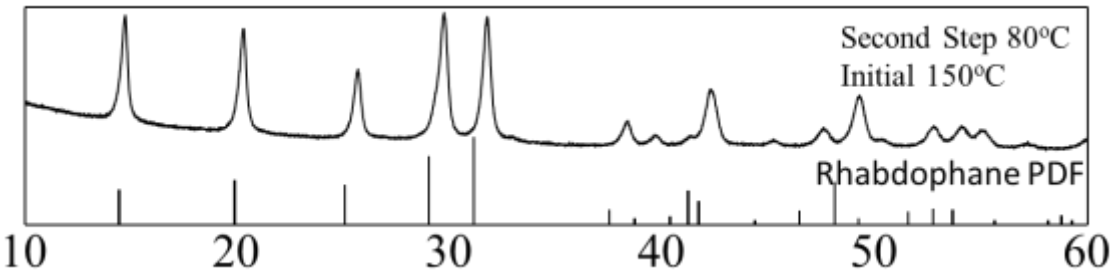

Fig. 1.21: XRD spectra of the second precipitation from the La-Dy separation after initial monazite precipitation of 150°C

1.2.5 Separation Factor

One way to quantify the amount of separation in a mixture of two constituents uses a distribution coefficient and a separation factor. The distribution coefficient usually refers to the concentration of a metal in an organic phase divided by the concentration of the metal in the liquid phase. In this case, the amount of the light rare earth incorporated into the monazite phasee was divided by the amount of light rare earth in the precipitant from the liquid pour off. An analogous expression can be made for the heavy rare earth. In these equations *m* is monazite and denotes that the compound from the first phase of the separation. *X* is xenotime and stands in for the second part of the separation as a subscript.

$$Distribution\ coefficiant\ D = \frac{[La_m]}{[La_x]} \qquad Eqn\ 1$$

To calculate the separation factor, the amount of light rare earth separated from the heavy rare earth, one divides the distribution coefficient of light rare earth by the heavy. Alternatively, the recovery coefficient of the light rare earth can be divided by the heavy rare earth (or visa versa) to get the separation factor.

$$Separation\ factor\ S_{La/Y} = {}^{D_{La}}/_{D_Y} \qquad Eqn\ 2$$

The afore mentioned math was used to calculate the separation factors in order to evaluate the systems presented in this report as well as compare to literature values.

Table 1.6: Separation factors calculated using residual La and Y

Monazite Precipitation T	residual Y in Monazite	Residual La in Xenotime	$S_{La/Y}$
200°C	10%	3.2%	3.36
175°C	10%	5.4%	1.94
150°C	8.9%	4.9%	1.89
125°C	5.5%	28%	0.15
100°C	6.8%	58%	0.05

1.2.6 Discussion of Rare Earth Separation by Different Phases Using Phosphoric Acid

The yields, or percent light rare earth recovered, observed in Table 1.1 show a generally decreasing trend with decreasing temperature. These slower kinetics would mean that in lower temperature solutions there is more La present in the decanted liquid going into the second phase of the separation. This observations suggests that higher temperature, or perhaps longer reaction times, should be more effective for separations. The more light earth elements that can be taken out of solution in the first step, the less there will be in the second step of the separation to incorporate the more valuable heavy rare earths as xenotime precipitant.

Crystal structure characterization of the initial powder by XRD matched the monazite structure at all temperatures shown in Figure 1.12. The peaks of the collected

powders were shifted to the right compared to the PDF card which suggests an increase in unit cell volume. This shift grows larger at high temperatures which was quantitated by rietveld refinement and reported in Table 1.2. If the larger Y ion was being incorporated substitutionally into the La monazite, it would follow that the unit cell volume would have to increase in order to hold the Y. Looking at each individual direction in the unit cell, there is no clear trend in the individual a b and c directions of the unit cell.

The second step of the separation the heavy rare earth Y was collected from decanted liquid left over from the first precipitation by heating in dilute conditions. The white powder collected was examined by XRD shown in Figure 1.14. A range of crystal structures were identified, from monazite to rhabdophane to xenotime. Note that the temperature of the second precipitation is always 80C which is too low to be at equilibrium conditions. This means any crystal that nucleates first would propagate instead of the most stable.

The yield of the initial monazite falls sharply with temperature, leaving quite a bit of La still in the liquid phase. This excess La prevents the formation of xenotime/churchite and preferred the faster forming monazite/rhabdophane structure. Even at higher temperatures we see the formation of monazite in the subsequent liquid separation when 60% of the La came out in the initial precipitation. At lower temperatures when there is much more La left over, only monazite or rhabdophane forms.

1.3 Rare Earth Separation by Homogeneous Precipitation Using Phytic Acid

1.3.1 Homogeneous Separation Methods

$La(NO_3)_3$ and $Y(NO_3)_3$ were dissolved in water to a 500x dilution in a 1L beaker shown in Figure 1.22. Phytic acid was added drop-wise to the mixed rare earth solution with stirring as shown in figure 2. White precipitation formed immediately. This was allowed to stir overnight without heating. Mixture was heated slowly to 100^{o}C at 10^{o}C/hour but no change was observed. The precipitant was then washed with water to pH 7, dried with acetone and characterized by SEM and XRD.

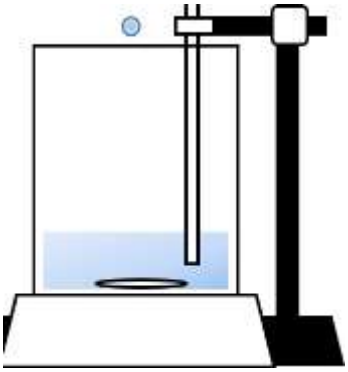

Fig 1.22: Phytic acid homogeneous separation experimental setup

The reaction was repeated with initial solutions of dilute $La(NO_3)_3$ and $Y(NO_3)_3$ separately, those reactions also produced white precipitant and were collected and washed. Diluted 10x phytic acid in water was also attempted and yielded similar results.

After initial characterization of powders, further analysis was carried out by annealing collected powders at 800^{o}C in a furnace for 5 hours. These processed samples were characterized by SEM and XRD.

1.3.2 Phytic Acid Results

After the diluted nitrates were added to the phytic acid, white precipitant formed immediately. This was collected and examined by XRD shown in Figure 1.23

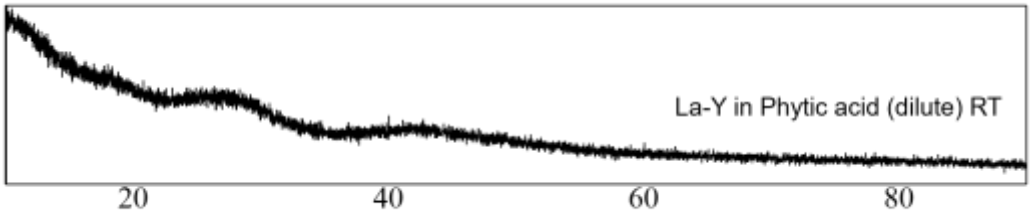

Figure 1.23: Mixed La and Y nitrate precipitated in phytic acid to produce amorphous white powder

The collected powder was examined by XRD and found to be amorphous. The ratio of La:Y in mixed rare earth precipitation was 1:3 by EDS. Figure 1.24 shows the lack of distinct morphology by SEM.

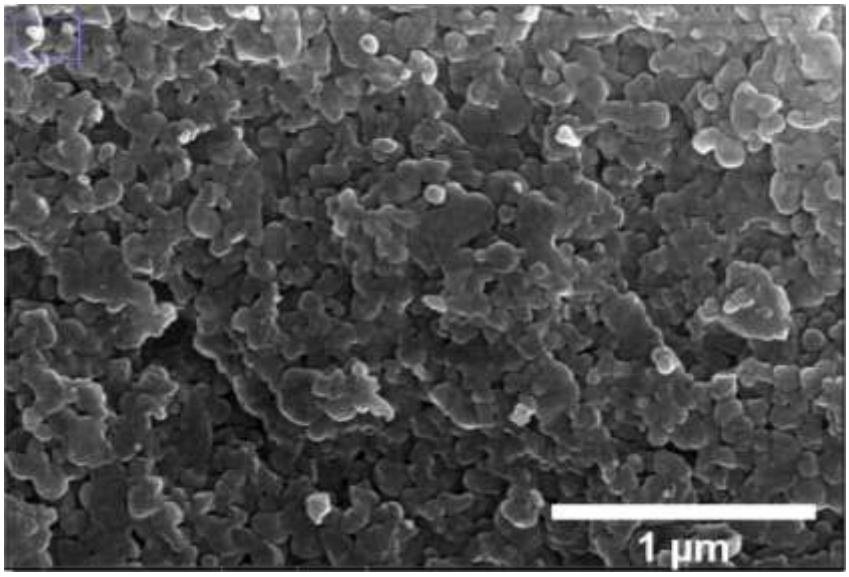

Figure 1.24: Amorphous La + Y phytic acid powder examined by SEM dispersed on Si wafer.

The powder was then annealed at 800^{o}C for 5 hours and XRD was taken. This time sharp peaks were observed in figure 1.24.

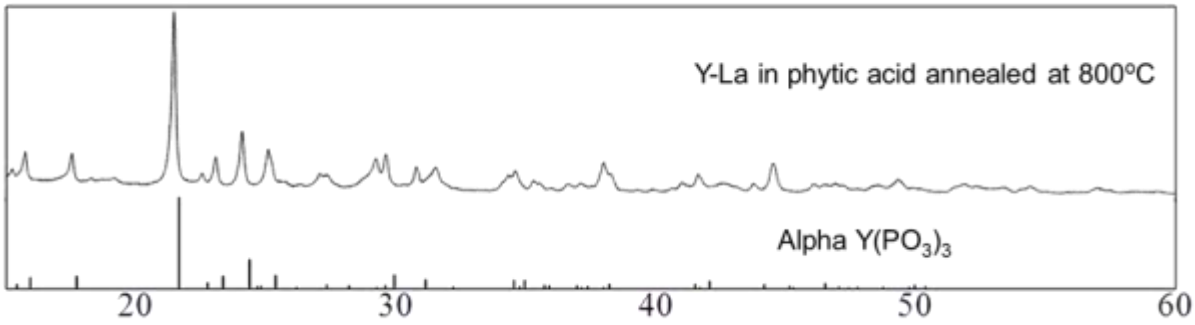

Figure 1.25: XRD of mixed Y and La in phytic acid after annealing for 5 hours at 800C. Peaks closely match alpha $Y(PO_3)_3$

To investigate further SEM was used to examine changes in the microstructure shown in Figure 1.25. Though the microstructure is less rounded and shows some plate like florets, it does not have a distinct morphology.

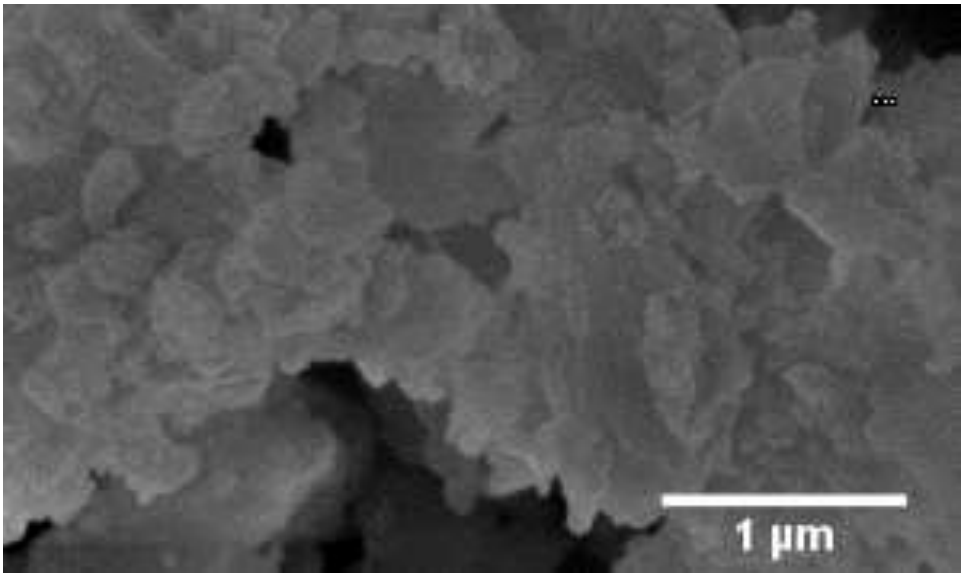

Figure 1.26: Mixed La + Y with phytic acid powder after annealing at 800°C for 5 hours on Si wafer under SEM

The Crystal structure was difficult to deconvolute so pure $La(NO_3)_3$ and $Y(NO_3)_3$ were mixed with phytic acid, washed and annealed as per the same procedure. After

annealing the two single rare earth phytic acid powders changed color observed in Figure 1.27, only the mixed Y and La rare earth powder stayed white.

Figure 1.27: Powders from phytic acid and rare earth nitrate reaction.

All powders were then examined by EDS in the SEM and are reported in Table 1.7. The atomic percents reported are normalized to the rare earth content. Oxygen content was discounted due to inherent inaccuracies so phosphorous and rare earth ratios could be compared.

Table 1.7: Measured atomic % of rare earth to phosphate ratios by EDS

	La + Y - Phytic	La - phytic	Y - phytic
	Atomic %		
La	1	1	0
Y	2	0	1
P	6	3	3

The XRD of $Y(NO_3)_3$ and phytic acid reaction was very similar to the mixture and matched yttrium polyphosphate $Y(PO_3)_3$ peaks as shown in Figure 1.28.

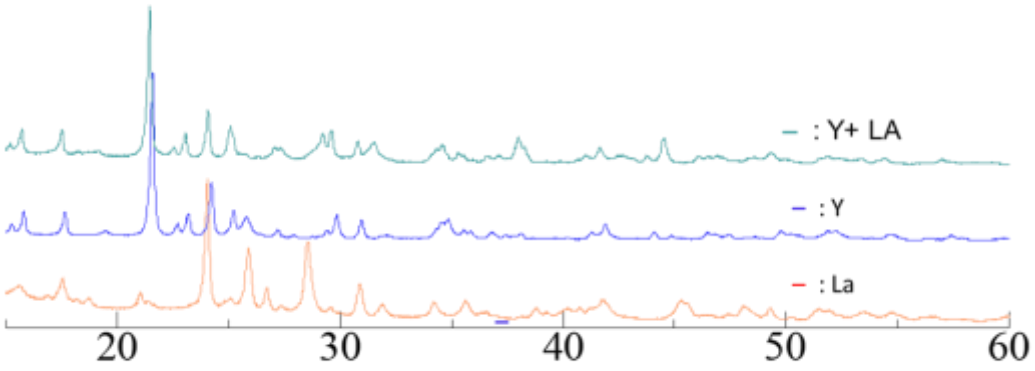

Figure 1.28: XRD of each phytic acid precipitation annealed for 5 hours at 800°C

While the mixed rare earths matched the Y phytic product ($(Y(PO_3)_3$), the La phytic product had a different crystal structure. The La nitrate and phytic acid mixture matched LaP_3O_9, a different polyphosphate shown in Figure 1.29.

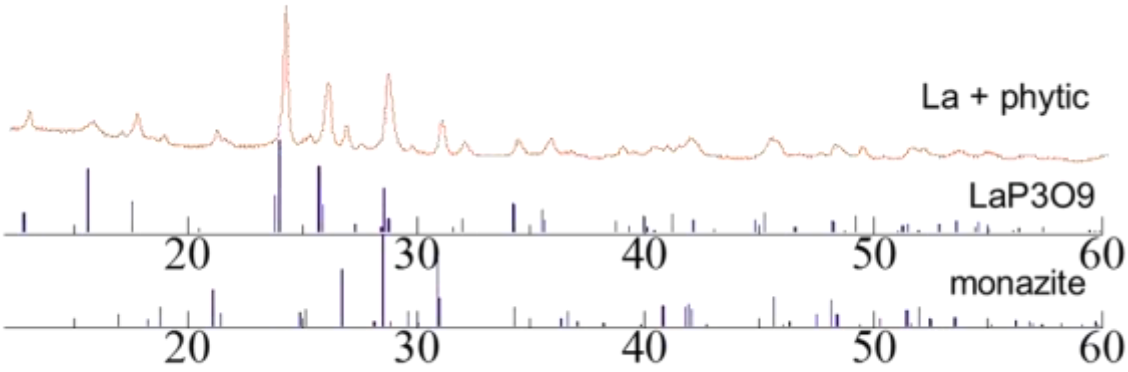

Figrue 1.29: Precipitant form the dilute La nitrate and phytic acid reaction after annealing at 800C compared to monazite and LaP3O9 PDF cards.

Looking back at Figure 1.28, the La + Y mixed phytic acid peaks and the Y phytic acid powder peaks are shifted to higher angles seen zoomed into the major peak in figure 1.30.

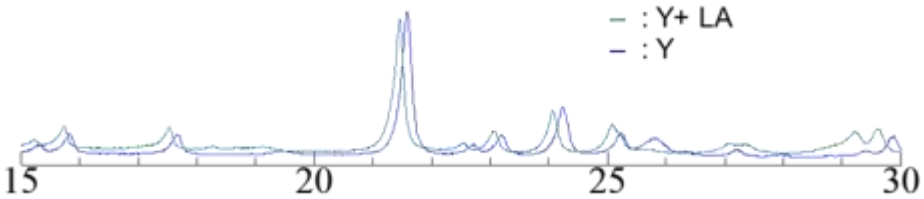

Figure 1.30: XRD of alpha $Y(PO_3)_3$ structure made from $Y(NO_3)_3$ and phytic acid compared to a mixture of Y and La nitrate.

The shift to the left in the mixture indicates an increase in the unit cell volume, as suggested by the comparison to the PDF card.

1.3.3 Phytic Acid Discussion

In order to precipitate anything from the rare earth nitrate solution in rare earths, it was necessary to have a dilute solution. This was thought to be due to the availability of the phosphate groups in aqueous conditions undergoing hydrolysis. This frees the phosphate ions to react with the rare earth nitrates which also disociate freely in solution. The speed

of the reaction was still unexpected. Both dilute phytic acid and dilute nitrates were attempted but had very rapid precipitation.

With the immediate precipitation appearing as white fluffy powder in suspension, it was not surprising to find out that it was amorphous in Figure 1.23. The two wide peaks at 25 and 42 degrees 2Θ did not match with previously common rare earth phosphate such as monazite or xenotime. The wide peaks could indicate a poorly crystalized precipitant. For example, later mentioned rare earth phosphate, LaP_3O_9, has a major peak around 25 degrees but there was not enough information in the spectra to confirm. Even with EDS data from table 1 the 3 to 1 ratio of La to Y did not help narrow down possible crystal structures.

To gather more information about the synthesised compound, it was annealed at 800C for 5 hours to coax out a more defined structure. The structure that was identified in figure 4. This was well matched to alpha Y(PO3)3 in the low angle region with some shift to higher angles compared to the PDF. At higher angles however some peaks did not match the intensities or were missing such as the extra peak at 45 degrees.

Further experiments with ony La nitrates and seperatly Y nitrates were carried out in hopes of furthering the understanding of the mixed La Y crystal structure. Figure 5 shows the XRD results of all of the mentioned experiments. From the comparison it is clear that in the presence of Y and phytic acid a yitrium phosphate structure is formed while La produces a lanthanum phosphate. Though they have different XRD the chemical structure and stoichiometry of the La phosphate and Y phosphate compounds are a similar 1:3 rare earth to phosphate which is backed up in Table 1.6.

As previously mentioned, the mixed rare earth phosphate compound's XRD has a shift towards lower angles compared to the PDF and just Y phosphate compound. This suggests an increase in unit cell volume to accommodate the larger lanthanum atoms. This method is not appropriate for the separation of rare earths as both La and Y precipitate in high amounts in the same phase.

It was observed that after annealing, the single rare earth phosphate compounds changed color. Initally all precipitants appeared as white powder after washing. However the La-phytic compound turned a light grey and the Y-phytic turned black. This is most likely due to the change in color center. The band of the Y phytic powder must have changed its band gap in annealing to nothing, making it possibly metallic. The grey could indicate an in-between transition similar to a semiconductor's band gap.

1.4 Conclusions and Future Work

1.4.2 Phosphoric Acid

Heavy and light rare earths have been separated into monazite and xenotime structures as well as others. Separation factors of 1.9 – 2.3 have been reported which corresponds to 95% - 97% purity of heavy rare earth material. The method presented is most similar to fractional crystallization which is inherently is cumbersome and laborious. This route has potential as a fast initial separation of mixed rare earth material, however commercial methods are much more efficient obtaining 99.999% purity with liquid extraction schemes.

1.4.2 Phytic Acid

Reactions of lanthanum and yttrium nitrate with phytic acid formed alpha-yttrium polyphosphate by XRD suggesting a preference for yttrium. Yttrium reactions with phytic acid showed the same structure with shifted peaks suggesting that lanthanum is incorporated into the structure. Examination by EDS showed approximately 35mol% of lanthanum in a pressed powder from the mixed reaction. This route was abandoned due to the low separation rates.

Ultimately, this experiment did not produce the results desired for an efficient separation of light and heavy rare earths. This experiment was designed with the intention of using a homogeneous precipitation method to slowly heat a mixture of rare eaths and collect them as they precipitated under different conditions. The instant precipitation upon addition of phytic acid prevents this method from being used this way. However if sodium

was added to tie up some of the phytic acid, the reaction might proceed more slowly. Time and resource constrains prevented this from being attempted.

CHAPTER 2: DIRECT PRECIPITATION FOR STOICHIOMETRICALLY BALLANCED $LaPO_4$ MONAZITE

2.1 Introduction

2.1.1 High Temperature Applications of Monazite

Lanthanum phosphate in the monazite structure has been of interest to a number of industries for its specialized set of properties. In the monoclinic structure oxygen has a nine-fold coordination around the lanthanum sites while the phosphorous has a four-fold coordination in a distorted tetrahedral environment shown in figure 2.1 [23]. Another possible structure of $LaPO_4$ is the hexagonal analog, rhabdophane $YPO_4 \bullet 2H_2O$ which can be converted by annealing at 800^oC . Most noticeable of its properties that arise due to its stable and unique structure are its high melting point (~2000K), low solubility in water and acids as well as a notably high resistance to radiation damage [24, 25, 26].

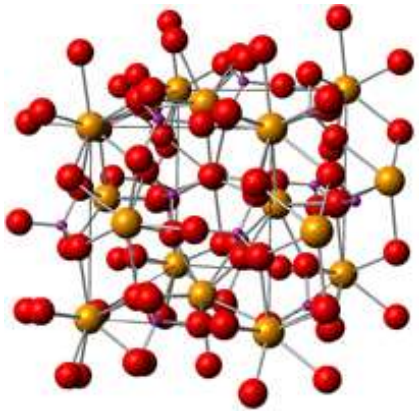

Fig. 2.1: Monazite $LaPO_4$ structure with 9-fold coordination red oxygen, and 4-fold yellow phosphorous and purple lanthanum

Monazite's properties make it a suitable material for a variety of applications. Its weak bonding properties allow it to be used as self-lubricant phase in diphase abradable

coatings as well as in fiber coatings and ceramic reinforced oxide composites as a toughening material [27]. The soft, easily machineable properties of $LaPO_4$ have been taken advantage of in order to make existing materials plyable by dispersing singe phase monazite in existing materials such as Al_2O_3 and ZrO_2 [28]. Its chemical stability and resistance to radiation make it useful in multiphase inert ceramic matrices in fuel and spent fuel waste management [29, 30, 31].

2.1.2 Monazite Synthesis Methods

Due to the extensive list of applications mentioned, numerous methods to make $LaPO_4$ monazite have been studied. Wet chemical method [32], sol-gel [33], high temperature solid state reactions [34], crystallization from phosphoric acid solution [35], and aqueous precipitation using $LaCl_3$ [36] have all been reported. Most of these methods involve long incubation times or multiple stages such as filtration, heat treatment as well as washing with hazardous chemicals. Some of these methods produce rhabdophane, the hexagonal hydrate crystal structure which must then be converted to monazite. This is especially problematic as the hexagonal structure is hypothesized by these authors to hold extra phosphorous in its needle like partial morphology even after conversion [37].

The direct precipitation of monazite, introduced by Schatzmann *et al.* [38] proposes a way to make $LaPO_4$ monazite without forming the undesirable rhabdophane intermediate. However, this method still produces excess phosphorus so the product must undergo washing with hazardous chemicals in order to produce clean monazite.

2.1.3 Monazite in High Temperature Applications

Within the collection of useful properties and uses, numerous applications lie within the high temperature industry, as should be expected with its high melting point. While examining the synthesis methods of monazite, one should keep in mind the phase diagram of the material in question, the relevant diagram for the La_2O_3/P_2O_5 system including the line phase $LaPO_4$, is presented in Figure 2.2 below.

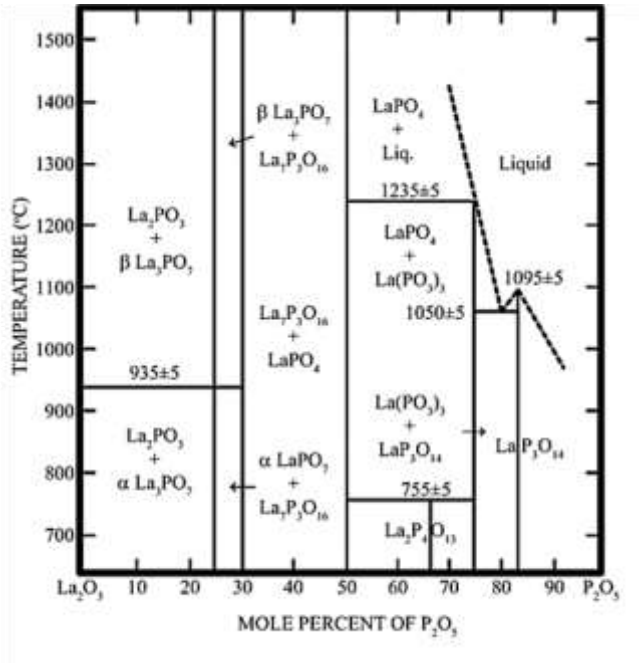

Fig 2.2. La_2O_3/P_2O_5 phase diagram [39]

The phase diagram reveals $LaPO_4$ to be a line compound. This is significant because divergence in ratios can lead to different phases forming. In particular excess phosphorus containing systems induce phase transformation to a peritectic liquid phase that forms around 1235°C. Further research using $LaPO_4$ and composite materials such as Al_2O_3 have shown that $AlPO_4$ can form in the presence of excess phosphorous and $LaAl_{11}O_{18}$ in the presence of excess lanthanum. [37] Forming extra phases in high temperature application

materials complicates and potentially weakens the system and thus is undesirable and even dangerous.

Previous studies have shown that even small amounts of excess phosphorous as low as 1wt% can have a detrimental effect on the microstructure stability and creep rates at high temperature [37]. This means that small changes in composition lead to much earlier failure. This is also a concern if $LaPO_4$ is to be considered for uses related to radionuclides; acid water could potentially dissolve the intergranular phases and weaken the material.

2.1.4 Objectives

The aim of the reported experiments is to synthesis stoichimetically balanced $LaPO_4$ monazite in a 1:1 ratio of La and P to negate the negative properties excess phosphorous lends to the material. It has been theorized that this could be done by starting with a limiting amount of phosphoric acid in balance with the lanthanum source, $La(NO_3)_3 \bullet 6H_2O$.

2.2 Methods for Stoichiometrically Balanced Monazite

In a water bath at 75 ±5°C, solid lanthanum nitrate hexahydrate (50 mg, 115 mmol, Alfa Aesar, 99.9%) were melted in a 250mL beaker. The setup of which is shown in Figure 2.3. While stirring, 85% phosphoric acid (J.T. Baker)(2.7mL, 45 mmol) was added drop-wise (10 drops per min). White precipitant formed immediately. After all the phosphoric acid was added the heat was turned off and the reaction was left stirring until it became too viscous. Precipitant was then washed with water until pH 6.5, then washed with acetone and dried. Product was examined by XRD and matched rhabdophane peaks. This was converted to monazite in a furnace at 800^{o}C for 10 hours. This was also examined by XRD to confirm conversion. A green body was made using cold Isostatic Press (CIP) in a mold (60% of $LaPO_4$ theoretical density). The green body was sintered at 1500^{o}C for 5 hours (92% of theoretical density) and polished using 600 girt, 5 um, 1 um, 1 nm for SEM.

In a sand bath at 75 ±5°C lanthanum nitrates (50 mg, 115 mmol, Alfa Aesar, 99.9%) were melted in a 250 mL beaker. While stirring, 2.7 mL of 85% phosphoric acid (2.7m, 45 mmol) was added drop-wise (10 drops per minute). The setup can be seen in figure 2.3. White precipitant formed immediately after the first drop of acid was added. After the acid was added the reaction was stirred for 3 days. Water was added to the reaction when liquid became too viscous to stir. Powder was collected and washed to pH6.5 then washed with ethonal, then acetone and dried at 80^{o}C in a crystallization dish. XRD showed monazite so no conversion set was necessary. A green body was made using cold Isostatic Press (CIP) in a mold (40% of $LaPO_4$ theoretical density). The green body was sintered at 1500 for 5 hours (80% of theoretical density) and polished using 600 girt, 5 um, 1 um, 1 nm for SEM.

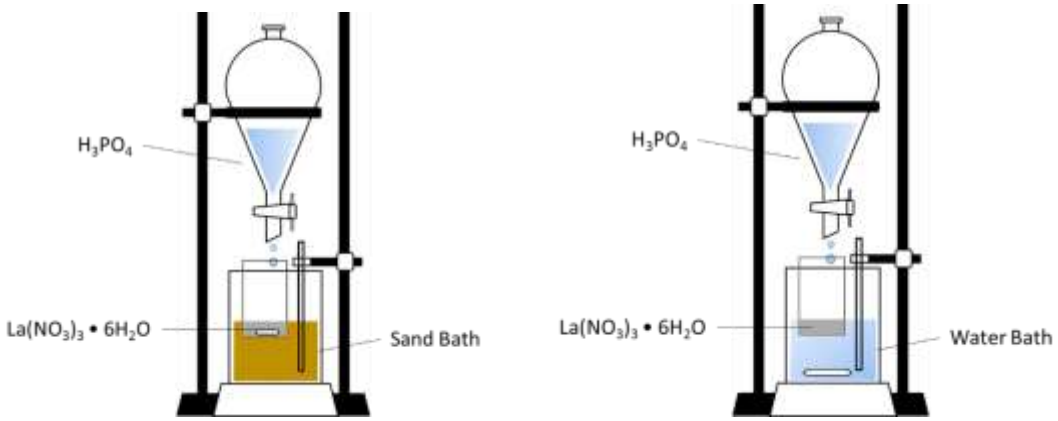

Fig. 2.3: Sand and water bath setups

Density was measured by geometry and weight after CIP and sintering. pH was measured by BDH pH Test 0-14, VWR International Radnor, PA USA. Crystal structures were evaluated via powder X-ray Diffraction using Rigaku Smartlab diffractometer, and Rietveld analysis with Cu-Kα x-ray source (λ= 1.5418 Å). The change in morphology and the secondary phase formed in the sintered samples were studied via secondary electron microscopy (SEM) imaging analysis using FES Magellan (400 XHR SEM). The SEM analysis was performed using an accelerating voltage range of 3-20 keV. Both powders and sintered samples were mounted on adhesive carbon tape, and were sputter coated with a thin layer of Iridium (Ir) to prevent charging during the imaging processes.

2.3 Results for Stoichiometrically Balanced Monazite

After each synthesis powders were collected and examined by XRD to deterime crystal structure. If rhabdophane was present it was necessary to convert it to monazite by annealing at 800°C for 10 hours. Figure 2.4 below shows the results from each synthesis method.

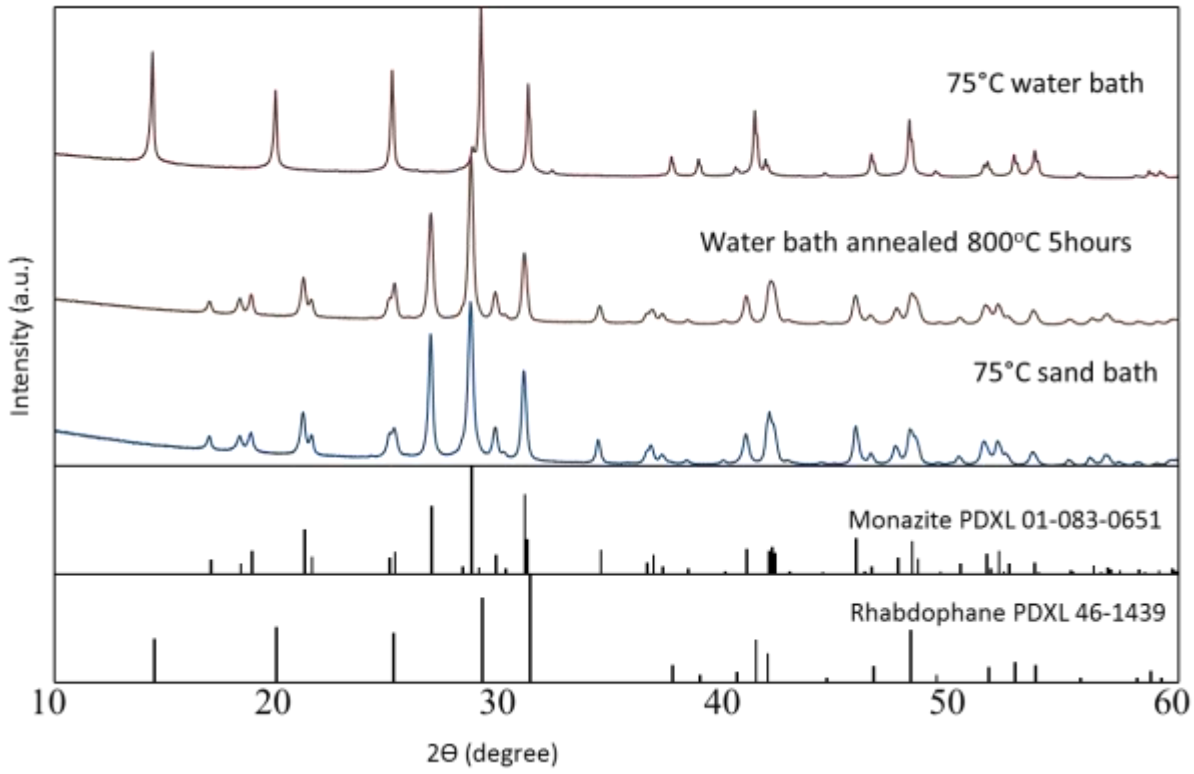

Fig. 2.4: XRD spectra of monazite synthesized at 75°C in a water bath, annealed at 800°C and 75°C in a sand bath compared to monazite and rhabdophane PDFs

Initially the water bath precipitation method with limiting phorphoric acid produced rhabdophane and thus had to be converted by annealing. After the annealing process it was fully converted to monazite, confirmed by XRD. The precipitant form the sand bath reaction matched monazite PDF card peaks completely, with no visible rhabdophane peaks.

After crystal structure had been confirmed, particles were examined by SEM for morphology and particle size shown in Figure 2.5.

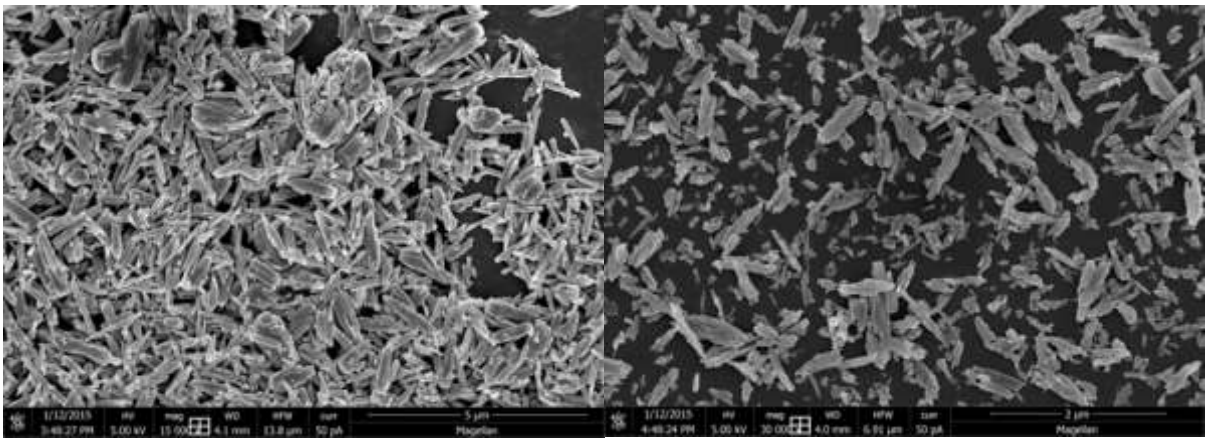

Fig. 2.5 A) Water bath and B) sand bath heating method initial precipitation SEM

The water bath method initial precipitation rhabdophane in figure 2.5a shows clustered, needle-like particles bundled together with an average particle size of about 900nm. Particles from the sand bath precipitation method showed a more plate-like morphology and a large range in particle size. There were scattered nanoscale particles and larger clusters of particles an average of about 360nm in size.

The examined particles were compressed into green bodies and sintered. The densified samples were cut and polished and examined under SEM seen in Figure 2.6.

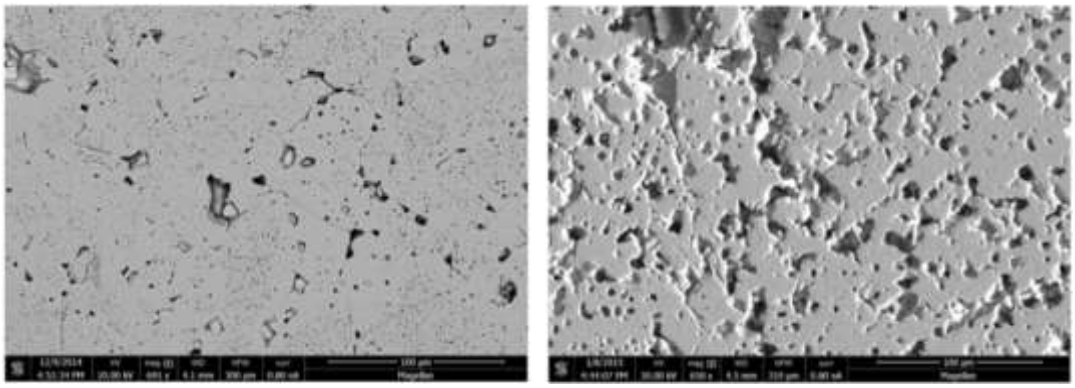

Fig. 2. 6: Backscatter SEM of water bath and sand bath heating methods after sintering

The polished cross sections clearly show that the water bath sample is denser than the sample made with the sand bath. Geometric density measurements report the densities as 92% for the water bath and 80% for the sand bath (relative to $LaPO_4$ full density). Tiny pores and thin lines are seen across the water bath sample compared to the large pores in the sand bath sample.

These samples were compared to commercial Stem and Aldrich powders after sintering shown in Figure 2.7 below after washing with ammonia.

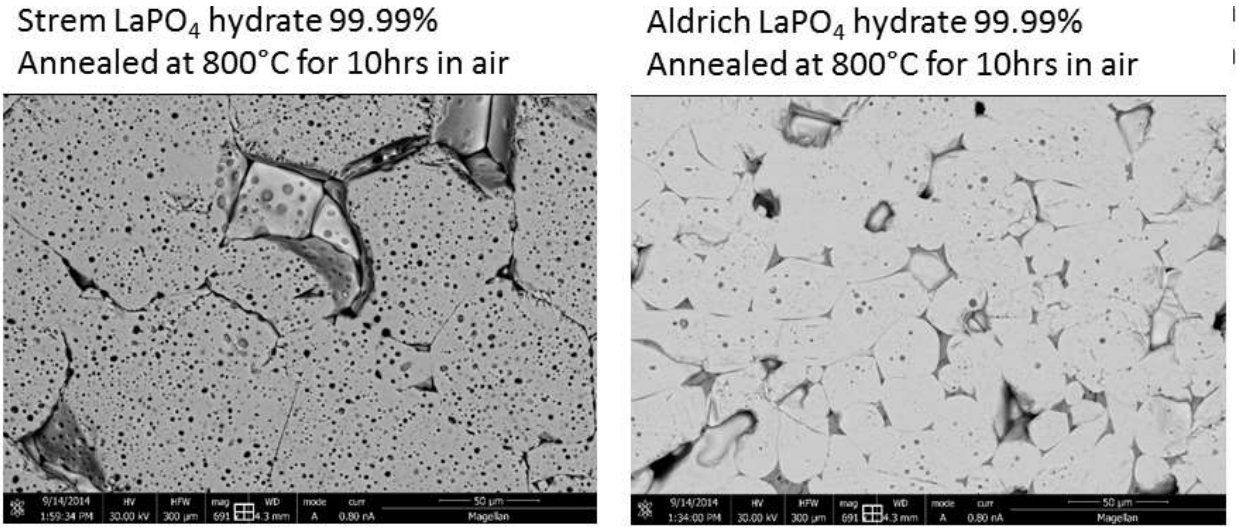

Fig. 2.7 SEM of Strem (left) and Aldrich (right) rhabdophane after annealing (800°C for 10 hrs) and sintering in air (1500°C for 2 hrs)

The LaPO4·0.5H2O from Aldrich contained excess P as an intergranular phase. The powder from Strem has a lot of dimples on the grains after sintering. Rapid grain growth was observed for Strem sample.

2.4 Discussion of Stoichiometrically Balanced Monazite

The direct precipitation method involving the addition of phosphoric acid to melted $La(NO_3)_3$ can either form rhabdophane or monazite shown in Figure 2.4 by XRD. The only difference between these reactions was intended to be the heating method, however there were inherent and necessitated differences between these methods.

One concern about adding phosphoric acid to the nitrates (Method II) instead of heating the phosphoric acid and adding nitrates drop-wise in liquid phase (MethodI), is the system cannot be heated to a high enough temperature to drive off the water. As the nitrate is not dissolved in water and water in phosphoric acid has been evaporated, there was minimal accessible water in the system, which should prevent the incorporation of water into the structure even at as low temperature as 70-80 °C. The temperature had to be kept at 70-80 °C to avoid solidification of nitrate and to keep the nitrate molten to stir the solution during the reaction. In the alternative method, minimum amount of phosphoric acid and excess nitrate were used. Thus, after the reaction there should only be excess La instead of P as in the direct precipitation method. Limiting the phosphorus source successfully prevented the formation of P-rich phase and did not require intense removal of excess P in the powder.

Phosphorous content was assessed visually by SEM backscatter images. Visually, Figure 2.6a shows some potential intergranular phase as triangular intergranular regions, 1-2um in size. In comparison Figure 2.6b shows large pores but no P-rich intergranular phase which would stand out as a dark region. The intergranular phase would be liquid at high sintering temperature, and it seems to wet the gain boundary in Figure 2.6a.

The commercial powders in Figure 2.7a and b show more wetting than sintered samples prepared by Method II. In particular the Aldrich sample shows significant wetting at grain boundaries.

2.5 Conclusions and Future Work

Different methods were used to synthase $LaPO_4$ monazite with a limiting amount of phosphoric acid with the aim of making “clean” stoichiometrically balanced product. Using the even heating of the sand bath to melt the precursor and dropping phosphoric acid into molten nitrates, synthesized $LaPO_4$ appeared to have less liquid phase than commercial powders by SEM without requiring washing with hazardous chemicals, strong bases such as ammonia.

REFERENCES

1. Meng, G.; Ma, G.; Ma, Q.; Peng, R.; Liu, X. "Ceramic Membrane Fuel Cells Based on Solid Proton Electrolytes." Solid State Ionics 2007, 178 (7-10), 697–703.

2. Nowick, a. .; Du, Y.; Liang, K. . "Some Factors That Determine Proton Conductivity in Nonstoichiometric Complex Perovskites." Solid State Ionics 1999, 125 (1-4), 303–311.

3. American Chemical Society National Historic Chemical Landmarks." Separation of Rare Earth Elements." http://www.acs.org/content/acs/en/education/whatischemistry/landmarks/earthelements.html (accessed May 23rd, 2016)

4. 4 Jones, Adrian P., Francis Wall and C. Terry Williams, eds. "Rare Earth Minerals: Chemistry, Origin and Ore Deposits, The Mineralogy Society Series #7", 1996, 372 pp

5. Gordon B. Haxel, Sara Boore, and Susan Mayfield from USGS; http://pubs.usgs.gov/fs/2002/fs087-02/ (accessed May 22nd, 2016)

6. Massari, S.; Ruberti, M. Rare Earth Elements as Critical Raw Materials: Focus on International Markets and Future Strategies. Resour. Policy 2013, 38 (1), 36–43.

7. Yunxiang Ni; Hughes, J. M.; Mariano, a. N. "Crystal Chemistry of the Monazite and Xenotime Structures." Am. Mineral. 1995, 80 (1-2), 21–26.

8. Carron, M. K.; Naeser, C. R.; Rose, H. J.; Hildebrand, F. a. Fractional Precipitation of Rare Earths with Phosphoric Acid. U.S. Geol. Surv. Bull 1958, 1036-N, 253–275.

9. Martini, A. "The Renaissance of Science: The Story of the Atom and Chemistry" 2014 Albert Martini

10. Atwood, A. D. "The Rare Earth Elements: Fundamentals and Applications" Dec 2014 Wiley

11. Pan, Z. W.; Weng, W. T.; Yan, H. B.; Yu, Y. L.; Wu, T. C.; Pan, J. D. Studies on Temperature Dependent Ionic Liquid Solid-Liquid Extraction Behavior of Rare Earth. Front. Manuf. Sci. Meas. Technol. Iii, Pts 1-3 2013, 401, 817–821.

12. Xie, F.; Zhang, T. A.; Dreisinger, D.; Doyle, F. A Critical Review on Solvent Extraction of Rare Earths from Aqueous Solutions. Miner. Eng. 2014, 56, 10–28.

13. Uda, T; Jacob, K. T.; "Technique for Enchanced Rare Earth Separation" Science 2000, 289, 2326 – 2329

14. Bonificio, W. D.; Clarke, D. R.; “Rare-Earth Separation Using Bacteria” Environ. Sci. Technol. Lett., 2016, 3 (4), pp 180–184

15. Schatzmann, M. T.; Mecartney, M. L.; Morgan, P. E. D. “Synthesis of Monoclinic Monazite, LaPO4, by Direct Precipitation.” J. Mater. Chem. 2009, 19 (32), 5720.

16. Lucas, S.; Champion, E.; Bregiroux, D.; Bernache-Assollant, D.; Audubert, F. Rare Earth Phosphate Powders RePO4·nH2O (Re=La, Ce or Y)—“Part I. Synthesis and Characterization. J. Solid State Chem.” 2004, 177 (4-5), 1302–1311.

17. Jonasson, R. G.; Vance, E. R. “DTA Study of the Rhabdophane to Monazite Transformation in Rare Earth (La-Dy) Phosphates.” Thermochim. Acta 1986, 108 (C), 65–72.

18. Kohlmann, H. Sowa, K. Reithmayer, H. Schulz “Structure of a Y1-x(Gd,Dy,Er)xPO4.2H2O microcrystal using synchrotron radiation”Acta Cryst., C50 (1994), pp. 1651–1652

19. Frost, R. L.; Lupez, A.; Scholz, R.; Xi, Y.; Filho, M. C. A “Vibrational Spectroscopic Study of the Phosphate Mineral Churchite (REE)(PO4)2H2O.” Spectrochim. Acta - Part A Mol. Biomol. Spectrosc. 2014, 127, 429–433.

20. Reddy NR, Sathe SK, Salunkhe DK (1982). "Phytates in legumes and cereals". Adv Food Res 28: 1–92.

21. Morgan, P. E. D.; Marshall, D. B. “Fiberous Composites Including Monazites and Xenotimes,” 1997.

22. Crea, F.; De Stefano, C.; Milea, D.; Sammartano, S. “Formation and Stability of Phytate Complexes in Solution.” Coord. Chem. Rev. 2008, 252 (10-11), 1108–1120.

23. D.F. Mullica, W.O. Milligan, & D.A. Grossie," Ninefold Coordination in LaPO4: Pentagonal Interpenetrating Tetrahedral Polyhedron". Inorganica Chim. 95, 231–236 (1984).

24. A. Meldrum, L. A. Boatner, & R. C. Ewing, "Displacive radiation effects in the monazite-and zircon-structure orthophosphates". Phys. Rev. B 56, 13805 (1997).

25. B. Glorieux, et al. "Study of lanthanum orthophosphates polymorphism, in view of actinide conditioning". J. Nucl. Mater. 326, 156–162 (2004).

26. J. M. Montel, J. Kornprobst, & D.Vielzeuf, "Preservation of old U-Th-Pb ages in shielded monazite: example from the Beni Bousera Hercynian kinzigites (Morocco)". J. Metamorph. Geol. 18, 335–342 (2000).

27. David B. Marshall, Peter E. D. Morgan, and Robert M. Housley." Debonding of Multilayered Composites of Zirconia and LaPO4". J Am Ceram. Soc 7, 1677–83 (1997).

28. S.S. Sujitha, S.L. Arun Kumarb, R.V. Mangalarajac, A. Peer Mohameda, S. Ananthakumara. "Porous to dense LaPO4 sintered ceramics for advanced refractories". 40, 15121–15129 (2014).

29. Danju Mena, Maulik K. Patelb, Igor O. Usovb, Moidi Toiammouc, Isabelle Monnetc, Jean Claude Pivind, John R. Portere, 1, Martha L. Mecartneya. "Radiation damage in multiphase ceramics". (2012).

30. G.J. McCarthy, W.B. White, D.E. Pfoertsch. "Synthesis of Nuclear Waste Monazites, Ideal Actinide Host for Geologic Disposal". Mat Res Bull 13, 1239–1245 (1978).

31. Dacheux, Nicolas; Clavier, Nicolas; Podor, Renaud. "Monazite as a promising long-term radioactive waste matrix: Benefits of high- structural flexibility and chemical durability". Am. Mineral. 98, 833–847 (2013).

32. S. Lucas, E. Champion, D. Bregiroux, D. Bernache-Assollant, & F. Audubert," Rare earth phosphate powders RePO4·nH2O (Re=La, Ce or Y)—Part I. Synthesis and characterization". J. Solid State Chem. 177, 1302–1311 (2004).

33. P. Chen, & T. Mah, "Synthesis and characterization of lanthanum phosphate sol for fibre coating". J. Mater. Sci. 32, 3863–3867 (1997).

34. Su, J. Zhou, & K. S. Shao," Reaction mechanism for the solid state synthesis of LaPO 4: Ce, Tb phosphor". J. Alloys Compd. 207, 406–408 (1994).

35. Kijkowska, "Preparation of lanthanide orthophosphates by crystallisation from phosphoric acid solution". J. Mater. Sci. 38, 229–233 (2003).

36. Lucas, E. Champion, C. Penot, G. Leroy, D. Bernache-Assollant, "Synthesis and characterization of rare earth phosphate powders". Key Eng. Mater. 206-213, 47–50 (2002).

37. Berbon, J. B. Davis, D.B. Marshall, R. M. Housley, P.E.D. Morgan, "High temperature creep of La-monazite". Int. J. Mater. Res. 98, 1244–1249 (2007).

38. Schatzmann, M. L. Mecartney, & P. E. D. Morgan, "Synthesis of monoclinic monazite, LaPO4, by direct precipitation". J. Mater. Chem. 19, 5720 (2009).

39. J. B. Davis, D. B Marshall, K. S. Oka, R. M. Housley, & P. E. D. Morgan," Ceramic composites for thermal protection systems". Compos. Part Appl. Sci. Manuf. 30, 483–488 (1999).